Paleoceanographic implications of diatom seasonal laminations in the Upper Miocene Pisco Formation (Ica desert, Peru) and their clues on the development of the Pisco Fossil-Lagerstätte.

Karen Gariboldi[1], Jennifer Pike[2], Elisa Malinverno[3], Claudio Di Celma[4], Anna Gionacada[1] and Giovanni Bianucci[1]

[1]Dipartimento di Scienze della Terra, Università di Pisa, Pisa, Italia.
[2] School of Earth and Ocean Sciences, Cardiff University, Cardiff, UK.
[3]Dipartimento di Scienze dell'Ambiente e del Territorio e di Scienze della Terra, Università di Milano-Bicocca, Milano, Italia.
[4]Scuola di Scienze e Tecnologie, Università di Camerino, Camerino, Italia.

Corresponding author: Karen Gariboldi karen.gariboldi@unipi.it, Dipartimento di Scienze della Terra, Università di Pisa, via Santa Maria 53, 56126, Pisa (Italia).

Keywords: mixed lamina-*Coscinodiscus* lamina duplet; permanent El Niño (El Padre); fall-dump; Western and Eastern Pacific temperature gradient; biogenic silica as upwelling proxy.

Keypoints:
- Laminae of the Upper Miocene diatomaceous Pisco Formation reveal that the fall dump mechanisms regulated marine primary production;
- The predominance of fall dump over upwelling implies a drop of the temperature gradient between the Western and Eastern Pacific;
- Evidences highlight a need of caution when using biogenic silica as a proxy for paleo upwelling.

Abstract

The detailed study of diatom laminations conducted by means of backscattered electron imaging (BSEI) serves as a powerful tool to unravel details of past ocean dynamics. In this paper we apply this method to the analysis of the diatomites of Cerro Los Quesos, Upper Miocene Pisco Fm, Peru. Numerous studies have been conducted on the Pisco Fm; however, a focus on its paleoceanographic significance is still lacking. In this work, we provide invaluable information on the oceanographic setting in the area at the time of diatomites deposition. The high abundance of deep-living *Coscinodiscus* laminae, proceeded by either a mixed lamina or a terrigenous one, let us hypothesize a deep position of the thermocline during the deposition of the Pisco diatomites; together with the scarcity of *Chaetoceros Hyalochaete* spp. resting spores, this evidence confutes the common belief that equals high biogenic silica content in marine sediments with enhanced upwelling in their area of deposition. Conversely, the depositional setting of the Pisco Fm diatomites is more similar to what is known as "permanent El Niño" (or "El Padre") state, meaning a constant weakened upwelling (or upwelling of nutrients-poor waters). Thanks to this study we also obtained refined information on the diatomites sedimentations rates. The comparison of the Pisco diatomites sedimentation rates with those of Quaternary diatomites, together with a consideration on the pore water content of the latter, gave strength to the hypothesis that the formation of the vertebrate Lagerstätte may have been enhanced, among others, by the so-called "impact-burial" mechanism.

Plain Language Summary

Some sedimentary rocks are formed by the remains of small organisms. This is the case of diatoms, which are microscopic algae with a siliceous exoskeleton. As we know the ecological conditions of the modern oceans in which different diatom species live, when we found them in sedimentary

rocks, we can infer the ecological conditions of the oceans millions of years ago. In this study, we present the species that we found in some Peruvian rocks, the so-called Pisco Formation, which dates back to 7/6 Million of years ago. Different species are preserved in these rocks in the same order in which they bloomed, so that we can identify one small "lamina" (an horizontal strip in the rock with a thickness smaller than 1 mm) for each blooming season. The species that we recognise are those that today bloom during "El-Niño", a particular climatic warm condition that today causes loss of large fishery stocks and inundations along the West American continent coasts and droughts in the inlands. This small finding helps us hypothesize how climate may evolve if the Earth's temperatures keep on rising. Also, as the rocks of the Pisco formation are famous because of their huge content of fossil whales and dolphins, the study of this rock helps us understand how this large mammals got preserved trough millions of years.

1. INTRODUCTION

The Late Miocene Pisco Fm, the youngest sedimentary unit filling the East Pisco forearc basin (Peru), is an exceptional marine vertebrate Lagerstätte (Lambert et al. 2010; Esperante et al., 2015; Collareta et al. 2015, 2021; Bianucci et al., 2016a and b; Gioncada et al., 2016; and references therein). We can get a glimpse of the importance of this Lagerstätte in terms of: 1) number of findings by citing the data reported by Bianucci et al. 2016a, b, where the authors report more than 300 specimens preserved as bone elements belonging mostly to cetaceans at the site of Cerro Colorado (Pisco Fossil Lagerstätte Ica Desert, Peru) and 192 fossils of marine vertebrates preserved as bone elements at Cerro Los Quesos (CLQ, Pisco Fossil Lagerstätte Ica Desert, Peru; Fig. 1A, B); 2) the exceptional preservation of the specimens, both in terms of completeness and details of delicate features such as baleens (e.g., Esperante et al., 2015; Bosio et al., 2021b; Collareta et al., 2021), and; 3) the scientific relevance of this findings by recalling that the Miocene represents a pivotal moment in the evolution of marine vertebrates (Marx and Uhen, 2010).

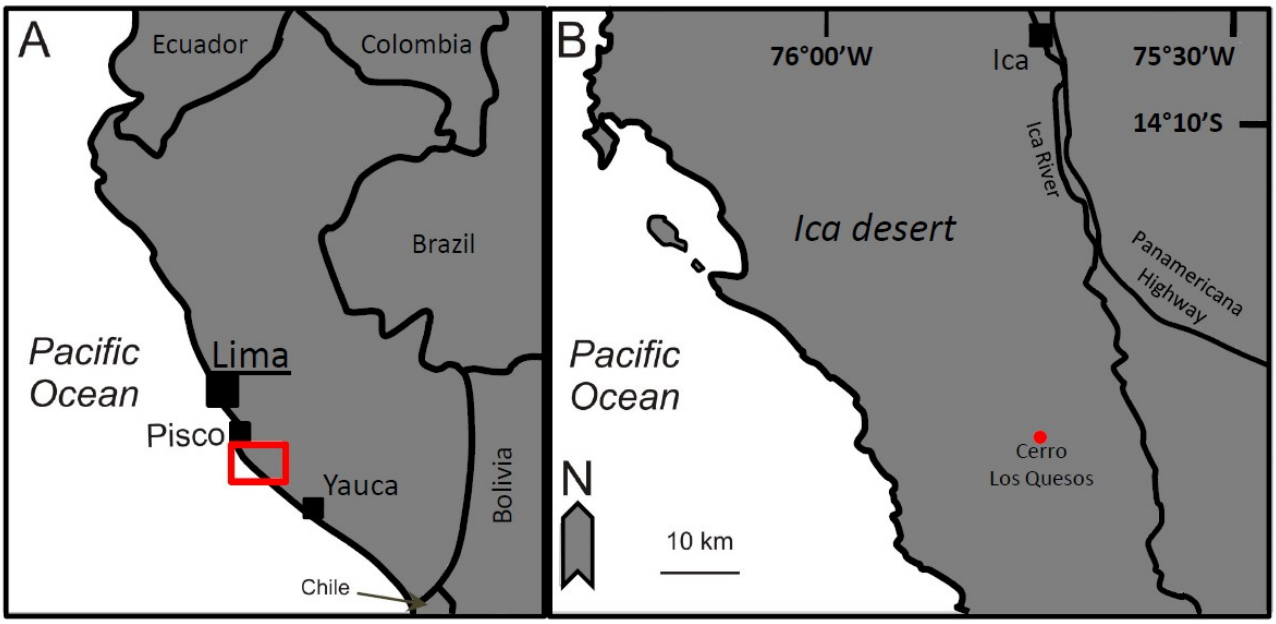

Figure 1. Geographic setting of the Ica desert. A. Sketch map of Peru, with location of the Ica desert (red square). B. Close up of the Ica desert; location of Cerro Los Quesos (CLQ).

Recently, researches have not only dealt with the evolutionary and taxonomical aspects of the fossil specimens of the Pisco Lagerstätte, but also with the mechanisms that have favored the fossilisation of all these organisms. Brand et al. (2004) and Esperante et al. (2008, 2015) were the first to hypothesize some of the mechanisms that may have led to the development of the Lagerstätte, citing early mineralisation of the carcasses due to the rapid burial and sedimentation

rates in the Pisco Fm two to four orders of magnitude higher than in modern analogues. However, only some more recent papers (Gariboldi et al., 2015, 2017; Gioncada et al. 2016, 2018a, b; Bosio et al., 2021a, b) explored in detailed the cause of the rapid mineralisation of the carcasses and the sedimentation rates in the Pisco Fm. In particular, Gariboldi et al. (2017) were able to calculate the sedimentation rate of a stratigraphic section measured at CLQ, this being equal to 19±1 cm/ka. This estimate is high, but not exceptional if compared with sedimentation rates of other high productivity basins. However, we must underline that it was calculated using few tie points (either diatom bioevents or $^{40}Ar/^{39}Ar$ ages from volcanic ash layers). Considering this limit, we decided to expand our knowledge on the influence of diatom deposition on fossil preservation, by studying in detail the diatomaceous laminae characterising part of the stratigraphic section at CLQ. Such approach provides estimates of the annual sedimentation rates in the basin during the deposition of diatomites, by recognising the annual repetition of species blooms in the sediments: the thickness of annual sequences corresponds to the yearly sedimentation rates.

Previous high-resolution studies of laminated diatom-rich marine sediments have provided important insights into past seasonal cycles of phytoplankton productivity (Kemp et al., 2000; Pike et al., 2001; Stickley et al., 2005; Davies et al., 2009; Maddison et al., 2012; Pike and Stickley, 2013; Davies and Kemp 2016) by comparing the sequences of laminations with modern diatom seasonal assemblages obtained from sediment traps (e.g. Dunbar and Berger, 1981; Thunnel et al., 1993; Sancetta, 1995) in different environments, such as upwelling areas (Peruvian forearc basins: Kemp, 1990, Brodie and Kemp, 1994; Gulf of California: Pike and Kemp, 1996b, 1997, 1999; Santa Barbara Basin: Bull et al., 2000), enclosed seas, as the Mediterranean Sea (Kemp et al., 1999; Corselli et al., 2002) and Black Sea (Pilskaln and Pike, 2001), the Southern Ocean (Grigorov et al., 2002; Alley et al., 2018; Tesi et al., 2020).

In their study on Pleistocene laminae from the Santa Barbara Basin, Bull et al. (2000) were able to recognise evidence of El Niño events. These were reflected in the frequency of terrigenous laminae representing the continental runoff caused by the intensified rainfall associated to this phenomenon. In the coastal water of Peru, the modern El Niño Southern Oscillation (ENSO) causes a warming of the subsurface water and the consequent deepening of the thermocline (e.g. Caviedes, 1984). This condition modifies the regular Peruvian upwelling regime, by preventing the south-easterly winds to act on the deep cold and nutrient-rich waters segregated under the deeper thermocline. As a consequence, primary production in surface waters declines, causing the loss of large fishery stocks, inundations along the coast and droughts in the inlands (e.g. Caviedes, 1984).

El Niño Southern Oscillation-like variability has been observed in the laminated diatomites of the Upper Cretaceous Marca Shale, California (Davies et al., 2012). Marty (1988) suggests that Eocene laminated diatomites from Fundo Desbarrancado (Southern Peru) testifies an upwelling regime already taking place during the Eocene. Most recent studies based on reconstructing the Pacific surface temperature measuring the Mg/Ca ratio on foraminifera tests have highlighted the presence of the El Niño phenomenon during the Pliocene (Ravelo et al., 2006, 2014 and references therein; White and Ravelo 2020a, b and references therein). These have suggested us that the study of the diatomaceous laminae of the Pisco Fm may have helped us found not only indications of the role played by the flux of diatoms to the sea bed in preserving the whale carcasses, but also of the climatic mechanisms that regulated the seasonal stratification of the water column in the area.

As such, although our information are limited to a small sample, in this paper we debate on the paleoclimatic significance of the CLQ laminae sequences and conclude presenting the implications that the sedimentation rates of the diatomaceous laminae had on the formation of the fossil Lagerstätte.

2. Materials and Methods

After numerous field campaigns undertaken between 2007 and 2015, a total of 192 fossil marine vertebrates were censed at CLQ in an area of approximately 4 km^2 (Bianucci et al., 2016b).

Information, such as the specimens' position, taxonomy, degree of completeness, degree of articulation and potential presence of dolomite nodule enclosing the bones were collected on dedicated sheets (Gariboldi et al., 2015).

The stratigraphic position of the fossils was based on the geological investigation and mapping carried out at CLQ by Di Celma et al. (2016). These authors subdivided the sedimentary succession exposed at CLQ in 6 informal lithological members that were labelled from A to F in stratigraphic order. The vertebrate census allowed to point out that 92.7% of the fossils are preserved in the "F member", which is composed mainly of a monotonous succession of finely laminated white diatomites (Di Celma et al., 2016). Considering that, due to the paucity of tie points, specific sedimentation rates were not calculated for each informal member (Gariboldi et al., 2017), in this study we try to identify seasonal laminae cycles in the F member to calculate the yearly accumulation rates of sediments into the basin during its deposition.

Using a metal conduit, a 25-cm-thick sample of laminated diatomaceous mudstone was collected in the F member of the CLQ stratigraphic succession, from under a vertebra of a fossil whale (Fig. 2A) called CLQ M58 (Fig. 2; hereafter M58. Specimen position: 14°30'58.3"S; 75°43'04.5"W; 167.0 m above the base of the measured section (abs), Bianucci et al., 2016b).

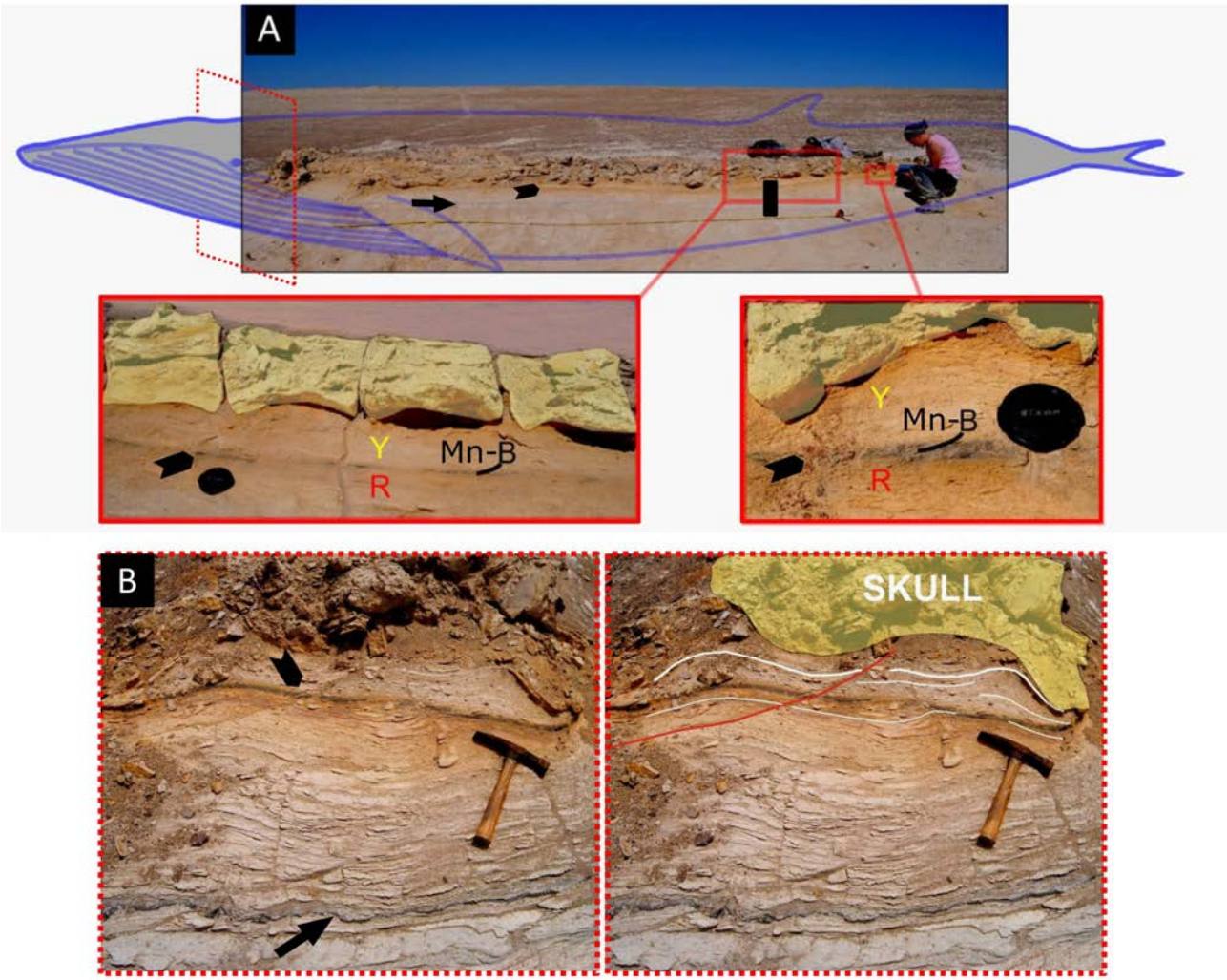

Figure 2. Fossil whale CLQ M58 (14°30'58.3"S; 75°43'04.5"W) at Cerro Los Quesos, Ica Desert, Peru. A. CLQ M58 in the outcrop. Black rectangle: location of the CLQ20 sample; black arrow: black tephra underneath CLQ M58 (not dated); black arrowhead: Mn layer of the YBR sequence (see text for explanation). The two red rectangles show the yellow portion of diatomites ("Y") underlain by a black manganese-rich layer ("B-Mn") and by reddish diatomites ("R") related to geochemical processes activated by the decomposition of the carcass (see Gariboldi et al., 2015; Gioncada et al., 2018). Camera dust cap for scale. The red dotted square highlights the position of Fig. 2B in respect to M58. 2B. Detailed of the diatomites below the skull of M58; right: the sedimentary features observed in the left picture are outlined. Laminations (white lines) are deformed by the weight of the skull (yellow area)

and in some points cut by the Mn layer (black arrowhead in the left picture). These deformations highlights that the carcass sank into the soupy, plastic diatomitic sediments as it reached the seabed. The geometry of the Mn layer with respect to the laminations shows that it precipitated after the diatomites were deformed. Red continuous line highlights secondary deformations. The black arrow points to the black tephra layer. Hammer as a scale. Modified from Gariboldi et al., 2015 and Bosio et al., 2021b.

The conduit was placed on the outcrop surface and sediments were excavated around the conduit profile. In this way, the conduit slid into the outcrop encapsulating the intact sediment section. Next, the protected sample was dug out of the outcrop. This technique facilitated the preservation of the 25-cm sequence and its stratigraphy. The sample was named CLQ20 (Fig. S1). Besides the fact that M58 is located in the F member, we decided to collect the sample for laminae analysis under it because: 1) M58 represents an almost complete and still articulated specimen, therefore representing a good example of exceptional preservation of the Pisco Lagerstätte; 2) the sediments directly underlying M58 are not only laminated, but also characterised by a typical sediment geochemical perturbation (the yellow-black-red sequence described by Gariboldi et al., 2015 and Gioncada et al., 2018a in the frame of the taphonomic studies of the Pisco Lagerstätte; see details of Fig. 2A) derived by diagenetic processes that bring to the precipitation of a dolomite nodule around the whale carcasses, therefore allowing us to have a complete frame of the different taphonomic processes that a carcass can undergo; 3) M58 is located on the top of the CLQ hill, on a morphological plateau that facilitates the access to the specimen, its observation and the sampling of the underlying sediments; 4) stratigraphically, M58 is placed between two dated volcanic ash layers: the older, the so called "Mono" ash layer, has an age of 6.93 ± 0.09 Ma, while the younger has a lower limit of ≥ 6.71 ± 0.02 Ma (Di Celma et al., 2016; See Note1 in Suppl.Mat.), therefore dating M58 and the CLQ20 sample back to the Messinian (Fig. 3).

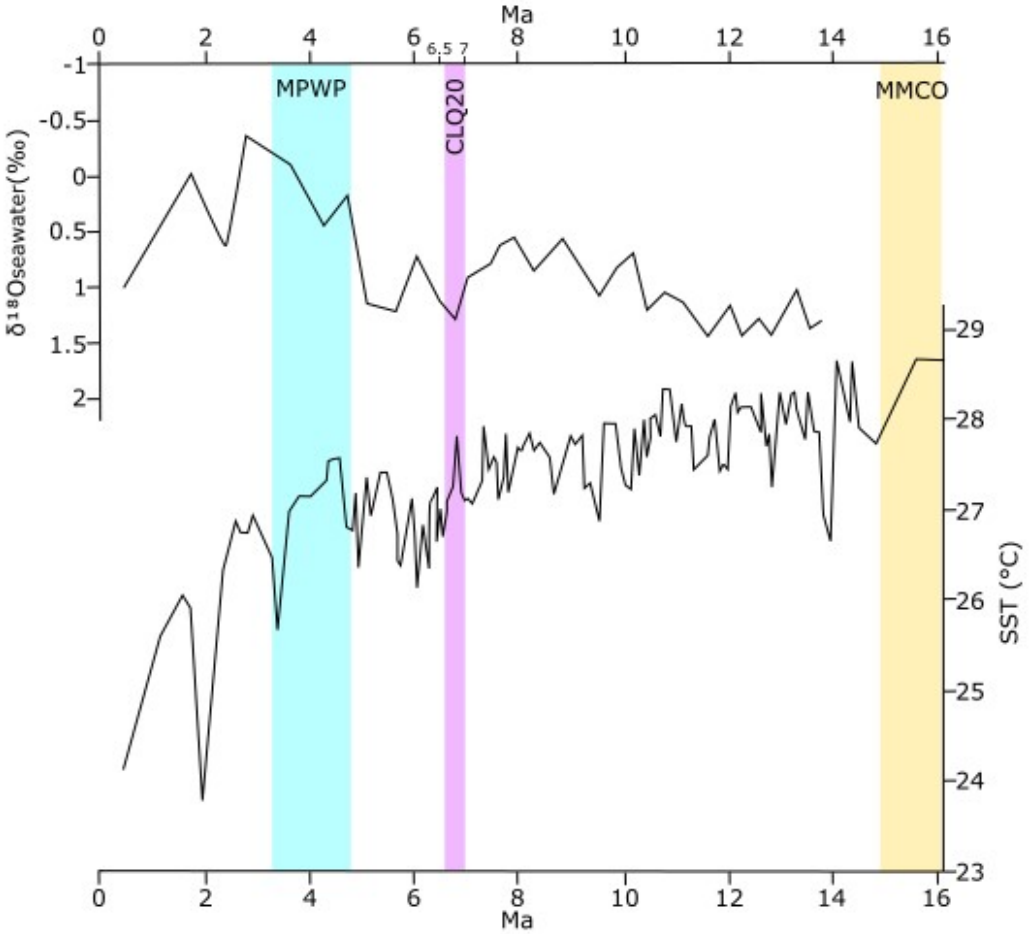

Figure 3. Temporal context of the CLQ20 sample. Sample CLQ20 was deposited between an older age limit of 6.93 ± 0.09 Ma, and a younger lower limit of ≥ 6.71 ± 0.02 Ma (purple square; Messinian), as suggested by two dated tephra in the CLQ stratigraphic

succession. The $\delta^{18}O_{seawater}$ (‰) and SST (°C) reported are those obtained by Rousselle et al., 2013 for the Eastern Equatorial Pacific (IODP Site U1338); SST are alkenone-derived, while $\delta^{18}O_{seawater}$ is reconstructed from the equation of Dudley et al., 1986 (see Rousselle et al., 2013). The light blue square and the yellow square represents respectively the middle Pliocene warm period (MPWP) and the Middle Miocene climatic optimum (MMCO). The CLQ20 sample dates back to a period characterised by high values of $\delta^{18}O_{seawater}$ and SST as high as during the WPWP. Modified from Rousselle et al., 2013.

Small, 4-5 cm subsamples of CLQ20 oriented perpendicular to the lamina fabric were embedded in epoxy resin (Araldite 2020) using a vacuum chamber and a total of 15 (Fig. S1) polished thin sections were prepared for scanning electron microscope backscattered electron imagery (BSEI) analysis (Kemp, 1990; Pike and Kemp, 1996a). Thin sections were carbon-coated and analysed in backscatter mode using a Veeco FEI -Philips- XL30 environmental scanning electron microscope in the School of Earth and Ocean Science, Cardiff University and a Hitachi TM 3030 SEM at the Department of Earth Sciences, Pisa University. One thousand two hundred and eighty-four BSEI images were taken to construct 20 BSEI photomosaics at 100x, 800x and 2000x magnification; and more than 400 high magnification images were collected. Only some selected images are presented in this work.

Laminations were described using 4 parameters: relative bimodality, laminae content (terrigenous or biogenic particles, diatom species composing each lamina), laminae boundaries (straight or wavy, sharp or blunt) and laminae lateral continuity.

The relative bimodality is, as described by Grimm et al. (1996), the relative difference in gray value between adjacent laminae. However, differing from Grimm et al. (1996), we evaluated the bimodality from the BSE images and not from X-radiograph. The difference in gray value on a BSE image depends on the atomic number of the element hit by the electron beam. Terrigenous particles have a higher atomic number than the epoxy resin filling the pores of diatoms and therefore appear lighter. As such, as stated by Grimm et al. (1996), high bimodality (HB) couplets are more evident where pure diatomaceous ooze laminae juxtapose terrigenous laminae. Conversely, low bimodality couplets (LB) are made of discernible laminae but with a very low gray contrast (as in the case of two diatomaceous laminae bearing different species associations). An intermediate situation between HB and LB is defined as moderate bimodality (MB).

3. Results

3.1. The CLQ M58 Whale and the CLQ20 Sample: in Situ and Macroscopic Observations

The M58 whale is an indertermined Balenopteroidea censed by Bianucci et al. (2016b) in the F member of the sedimentary succession exposed at CLQ and described as an articulated skeleton with the skull eroded (Table 1 of Gariboldi et al., 2015 and Fig. 2A, B of this work). M58 lies on a yellow portion of diatomites underlain by a black manganese-rich layer and reddish diatomites (Fig. 2A, B, black arrowhead) related to geochemical processes activated by the decomposition of the carcass (see Gariboldi et al., 2015; Gioncada et al., 2018a; see in particular paragraph 3.5 and Fig. 5 for explanations). Therefore, we consider the Mn layer as the boundary between sediments influenced by the presence of the carcass (sediments above the Mn layer) and those not influenced by its presence (sediments below the Mn layer). Below the reddish layer the diatomaceous mudstone shows millimetric white-to-dark grey laminations. The CLQ20 sample represents the sediment under M58 from the yellow diatomites to the gray laminated diatomaceous mudstones, which are interrupted near the bottom of the sample by a 5 mm-thick black tephra (Fig. 2A, B, black arrow); unfortunately, the latter could not be dated because of the lack of both biotite and sanidine crystals.

Detailed field observation of the skull of M58 highlighted that the lamination was deformed and in some points cut by the Mn layer (Fig. 2B). This deformation strongly resembles the shape of the side of the skull lying on the diatomites and, as suggested by Bosio et al. (2021b), could be the

evidence of the sinking of the carcass into the soupy but plastic diatomitic sediments as it reached the seabed.

3.2. Sediment Bimodality, Laminae Content, Styles, Sequences, and Laminae Thicknesses

Visual analysis of the low magnification mosaics (100 x) was used to give a general evaluation of the bimodality pattern of the sediment. The sediment appears to be mainly characterized by low to moderate or moderate bimodality (L-MB or MB; Figs. 4A; 5A; 6A; 7A), which is mostly given by the sparse presence of silt particles. Silt particles appear very light in BSE images, within a dominant dark matrix made of the siliceous diatom frustules (Figs. 4C, D, G, J; 5C, D, E, F, H, J, L, M; 7D, E, F; 8G, H). Only rarely the bimodality is high (HB) and this condition is always verified where the terrigenous components dominated by clay particles are grouped to form laminae overlying and overlaid by biogenic ones (Figs. 6A; 7A; 8A).

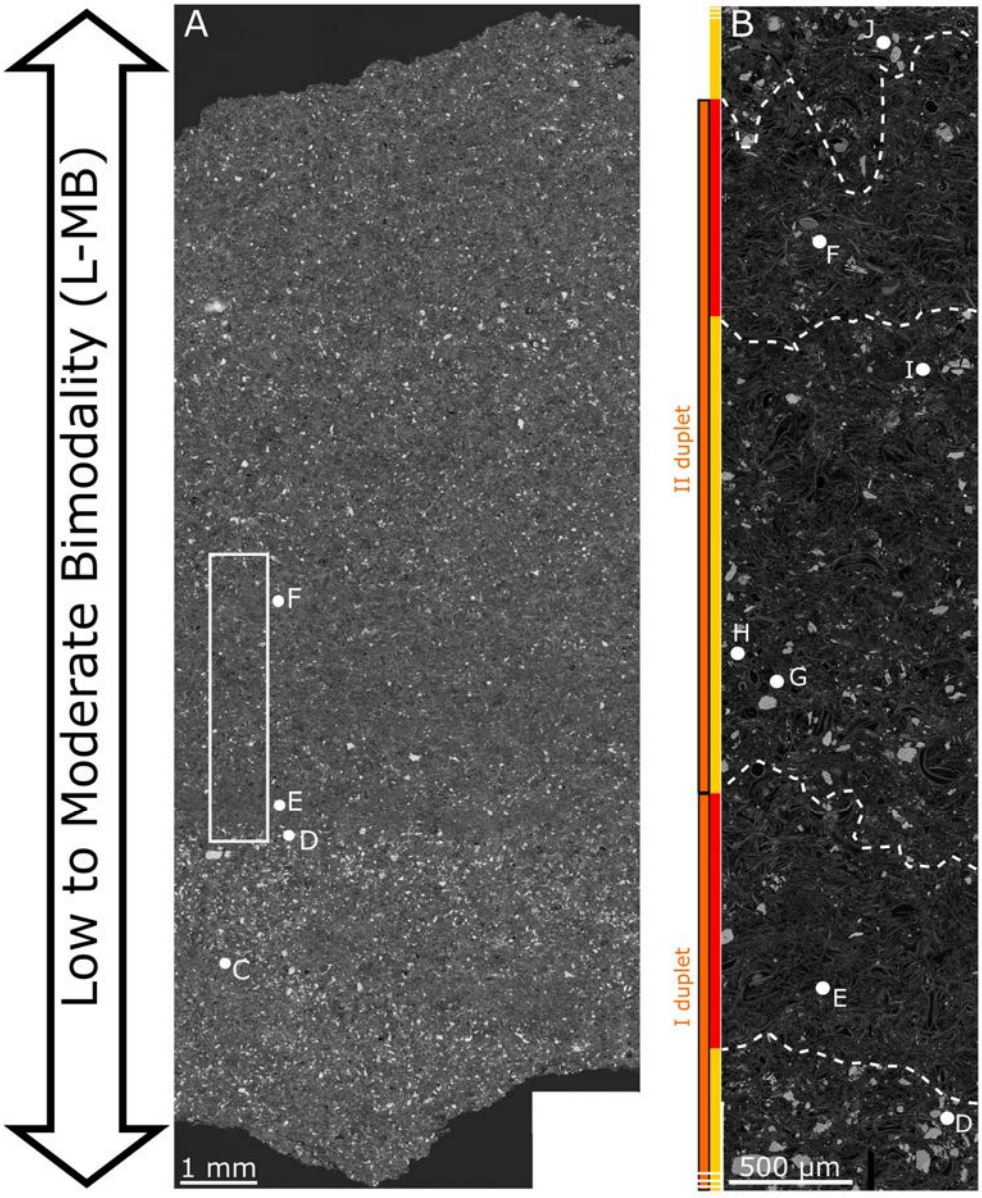

Figure 4 part I. BSE-SEM images of slide t13. A. Low magnification (100x) BSE image of slide t13, which is characterised by a low to moderate bimodality (L-MB). This bimodality pattern is mostly given by the sparse presence of silt particles within a darker matrix

(diatomite). The white rectangle indicates the position of 4B; letters highlights the same spots in 4A and 4B as well as Figure 4 part II. The mixed lamina (yellow rectangles) - *Coscinodiscus* lamina (red rectangles) duplets (orange rectangles) are discernible. Mixed laminae are particularly recognizable due to the presence of silt particles. Boundaries between laminae (white dotted lines) are wavy and indistinct. Coloured rectangles are dotted when laminae are not pictured in their whole length.

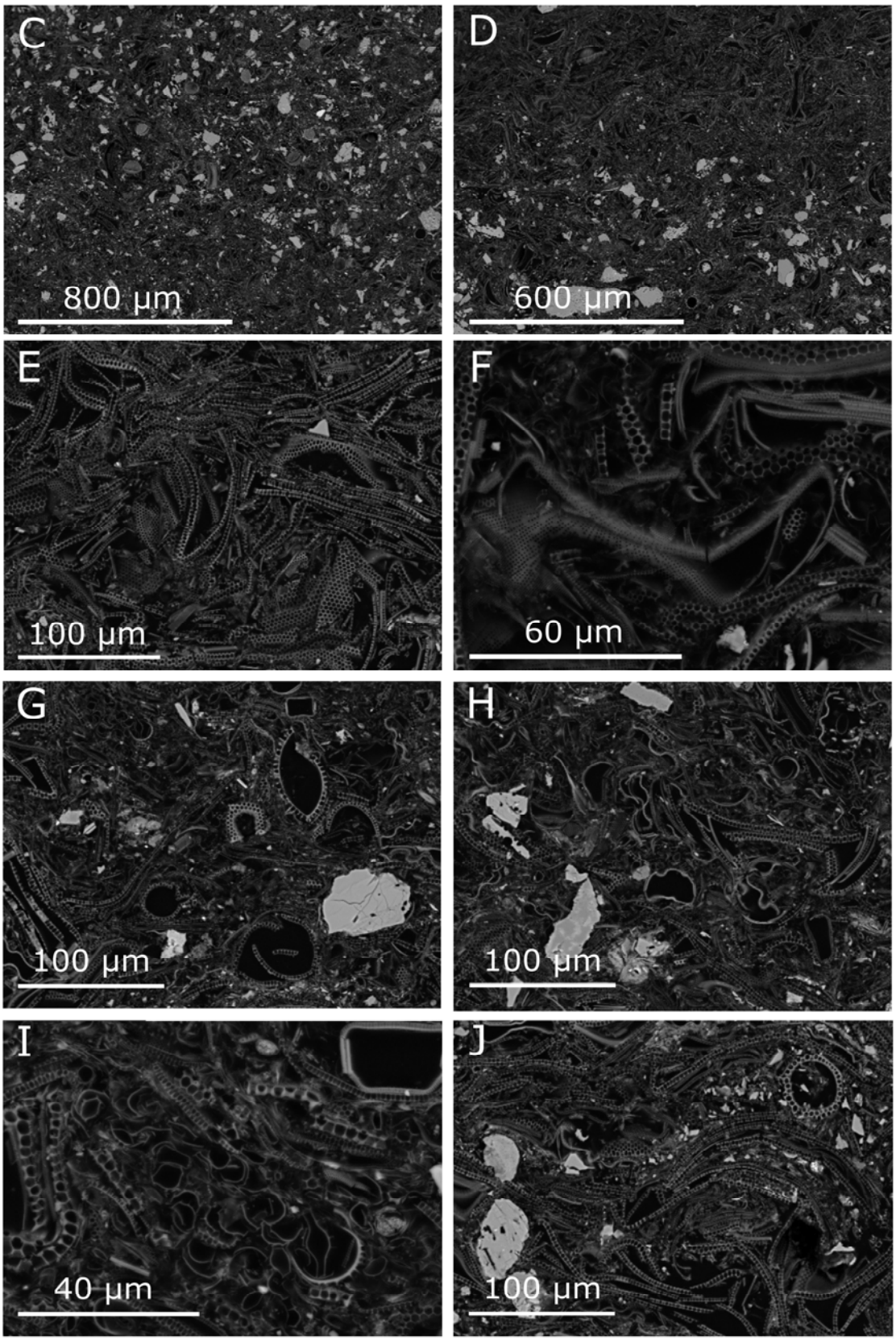

Figure 4 part II. Details of slide t13. C. Silt particles in mixed lamina. D. Boundary between a mixed lamina (bottom) and a *Coscinodiscus* lamina (top). E. Detail of *Coscinodiscus* frustules in a *Coscinodiscus* lamina. F. Detail of *Actinocyclus octonarius*

frustules in a *Coscinodiscus lamina*. G. Detailed of a mixed lamina; silt particles, *Stephanopyxis* frustules and *Actinoptychus* frustules are visible. H. Detailed of *Actinoptychus* frustules in a mixed lamina. I. A bunch of *Chaetoceros Hyalochaete* resting spores in a mixed lamina. J. Detail of a mixed lamina: silt particles, *Coscinodiscus* frustules and *Stephanopyxis* frustules are visible.

On the basis of the laminae content we can identify:

- terrigenous laminae: laminae where terrigenous particles are > 90% of the laminae. In CLQ20 these laminae are mostly made by clay particles (Figs. 6B, E; 7B, C, F; 8D, E, F), but also some silt particles (Figs. 8A, D) or biogenic particles, such as rare *Thalassionema* specimens (Fig. 6C), or other species (Fig. 8D).

- *Coscinodiscus* laminae: in this paper we use the definition "*Coscinosdiscus* lamina" to indicate a diatomite (a hard pelagic sediment made by >30% of skeletal remains of diatoms and <30% silt and clay, as defined by Palmer et al., 1986) where *Coscinodiscus* is the dominant genus (>90%; figs. 4B, E; 5B, F, G, I, K, M; 8A, C, G). Other rare components of these laminae are *Actinocyclus octonarius* specimens (Fig. 4F), *Thalassionema* specimens (Fig. 8B) and rare terrigenous particles (Fig. 4E).

- Mixed laminae (Figs. 4A, B, G, H, I, J; 5A, B, C, D, E, H, J, L; 6A, B, C; 7A, D, E, F; 8A, H): these are laminae composed of clay and silt particles in different percentages (Figs. 4B, C, D, G, I; 5B, C, D, E, H, L, N, O; 6C; 7D, E, F; 8A, H), specimens of *Coscinodiscus* (Figs. 4B, J; sometimes the presence of *Coscinodiscus* in mixed laminae is due to an interdigitation of *Coscinosidiscus* laminae with mixed laminae as in Fig. 5N) *Actinoptychus* (Figs. 4H; 5D, red circle), *Stephanopyxis* (Figs. 4G, J; E, red circle) and *Chaetoceros Hyalochaete* spp. resting spores (CRS; Figs. 4I; 8I). The percentages of these different components vary in each mixed lamina.

- *Actinoptychus* laminae: rare diatomites where *Actinoptychus* represents >90% of the diatom genera (Figs. 6A, D, E).

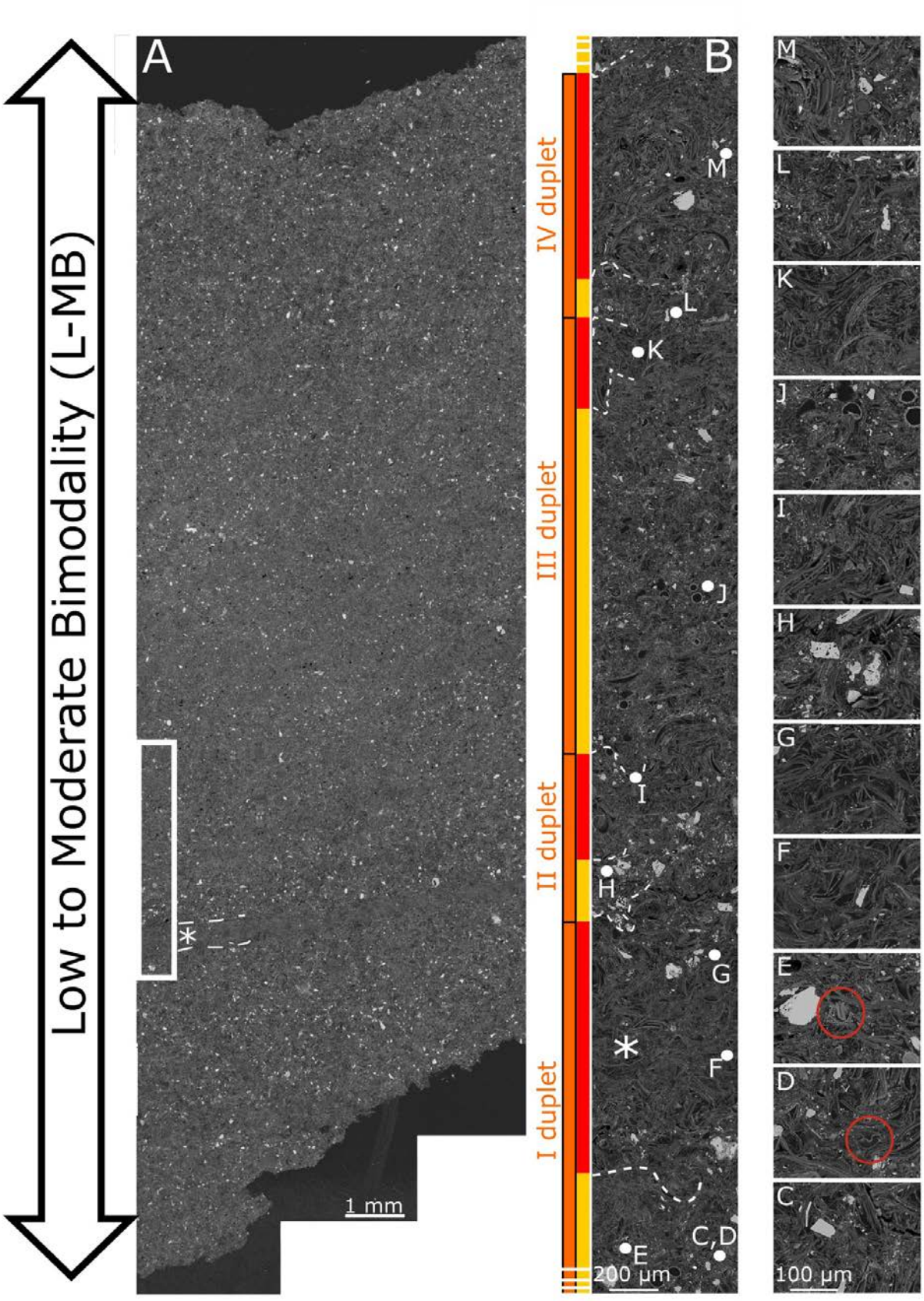

Figure 5. BSE-SEM images of slide t14. A. Low magnification (100x) BSE image of slide t14, which is characterised by a low to moderate bimodality (L-MB). This bimodality pattern is mostly given by the sparse presence of silt particles within a darker matrix (diatomites). The white rectangle indicates the position of 5B, while the asterisk highlights the position of a *Coscinodiscus* lamina particularly evident even at low magnification (this lamina is visible also in 5B and 5F; dotted lines outlines part of the *Coscinodiscus*

lamina boundaries, which are wavy, quite distinct and continuous. B. 800x magnification of slide t14; four mixed lamina (yellow rectangles) - *Coscinodiscus* lamina (red rectanlges) duplets (orange rectangles) are discernible, but the lowest one lacks the bottom of the mixed lamina. The sequence represented in 5B ends with the bottom of a mixed lamina (yellow rectangle). Coloured rectangles are dotted when laminae are not pictured in their whole length. The mixed lamina – *Coscinodiscus* lamina duplets have thickness varying form 625 µm to ca. 1750 mm, with a huge difference in the thickness of the two mixed laminae (ca. 375 µm in the second duplet vs. ca. 1500 µm in the third duplet). The *Coscinodiscus* lamina of the second and third duplets have more similar thicknesses (ca. 250 µm) but the *Coscinodiscus* lamina of the first and fourth duplets are ca. 1000 µm thick (thickness of laminae are approximate as their thickness vary along their length). Letters highlights the position of images in the right column. C. silt particles in a mixed lamina. D. *Actinoptyhcus* frustule in a mixed lamina (circled in red). E. Silt particle and *Stephanopyxis* frustule (circled in red) in a mixed lamina. F, G. *Coscinodiscus* frustules and silt particle in a *Coscinodiscus* lamina. H. Silt particles and *Coscinodiscus* frustules in a mixed lamina. I. *Coscinodiscus* lamina at its upper boundary with a mixed lamina. J. *Stephanopyxis* frustules and silt particles in a mixed lamina. K. *Coscinodiscus* frustules in a *Coscinodiscus* lamina. L. Silt particles and *Coscinodiscus* frustules in a mixed lamina. M. *Coscinodiscus* frustules and silt particle in a *Coscinodiscus* lamina. The 100 µm scale bar is valid for figures 5C-M.

Straight lamina boundaries in sample CLQ20 are rarely found and difficult to be traced, as the transitions from one lamina to the next are often indistinct. More frequently, boundaries are wavy (Figs. 4B; 5B; 6D) and, as said, indistinct, especially when representing the limit between a diatomaceous lamina and a mixed lamina (Figs. 4A, B). Only in slide t14 quite distinct boundaries between a *Coscinodiscus* lamina and the over- and underlying mixed laminae are recognisable at low magnification (Fig. 5A, dotted lines). Noteworthy, the only sharp boundaries are those delimiting terrigenous clayey laminae from others (Figs. 6A, B; 7A; 8A). Boundaries between these laminae and the others are normally less wavy then those between biogenic laminae or straight (Figs. 6A -white arrows-; 7A; 8A); also clots of clay can be observed throughout some slides, resembling a terrigenous lamina, but having a boudinage-like aspect (Figs. 6A –arrowheads-; 7A – arrowheads and arrows on the right side of the figure-). We do not consider them laminae as they are very thin (also << 100 µm). These clots have very straight and distinct boundaries, just as terrigenous laminae (Figs. 7B, F).

Both composition and boundaries of laminae help in verifying if they are laterally continuous; in CLQ20, although boundaries are normally indistinct, they are normally continuous (Figs. 4A; 5A; 6A; 7A; 8A) and discontinuous laminae are present.

A deeper investigation at 800 x and 2000 x magnification helped the identification of different sequences of laminae, in particular:

- the mixed lamina-*Coscinodiscus* lamina duplet (Figs. 4B; 5B; S2)
- the terrigenous lamina-*Coscinodiscus* lamina duplet (Fig. 8A);
- the mixed lamina-*Actinoptychus* lamina duplet (Figs. 6A, D, E).

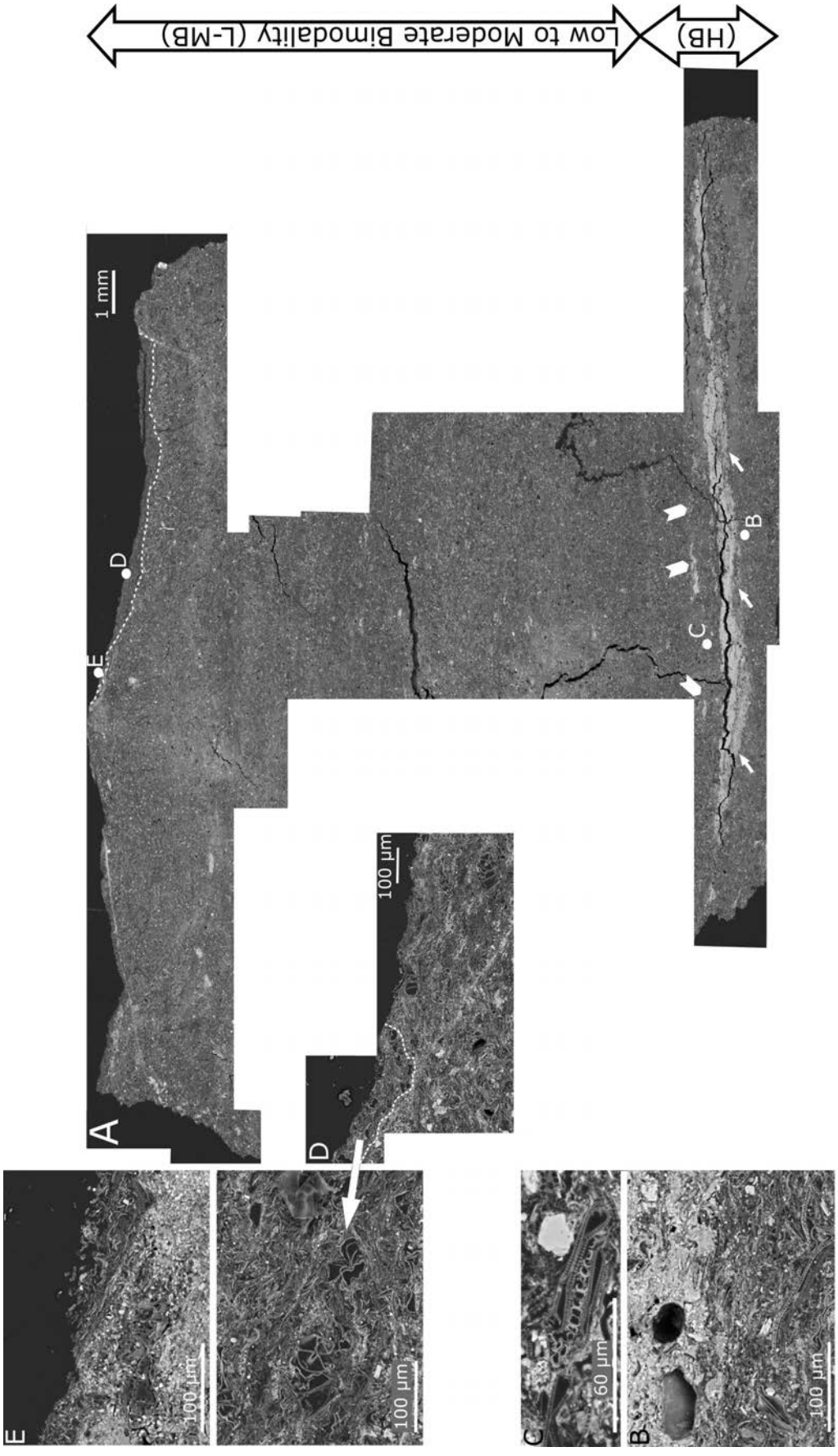

Fig 6. BSE-SEM images of slide t5. A. Low magnification (100x) BSE image of slide t5, characterised at its bottom by a high bimodality, given by the contrast of a terrigenous lamina and the terrigenous boudinage-like top of a mixed lamina (arrowheads) with the underlying and overlying biogenic laminae. The rest of the slide is characterised by a low to moderate bimodality (L-MB). This bimodality pattern is mostly given by the sparse presence of silt particles within a darker matrix (diatomite). White arrows at the bottom point to the lower boundary of the terrigenous lamina, which is straight to wavy but sharp. The dotted line at the top of the image highlights a wavy boundary between a terrigenous lamina and the overlying *Actinoptychus* lamina. Letters highlights the position of images in the left column. B. Detail of the lower boundary of the terrigenous lamina (the content of the underlying lamina is not defined, due to the imperfect polishing of the slide). C. *Thalassionema* specimens in the terrigenous lamina. D, E. Details of the boundary between the terrigenous lamina and the overlying *Actinoptychus* lamina; the white arrow in D points to an enlarged image of the *Actinopthychus* frustules.

The last case was observed only once and, therefore, it is considered rare. Also the terrigenous lamina-*Coscinodiscus* lamina duplet is evident only in one case (Fig. 8A). In Fig. 7A some clots of clay topping the mixed laminae can be observed (arrows on the right of the photo); these have a frequency of 3-3.5 mm, made exception for the first one, which is ca. 1 mm apart from the underlying terrigenous lamina. Similar clots overlying a mixed lamina are observed in slide t5 (Fig. 6A –arrowheads-, E).

Comparing at higher magnification (Fig. S2) the t9 slide (Fig. 7A) for its whole length it appears clearly that the sediment is mainly composed of the mixed lamina-*Coscinodiscus* lamina duplet, the mixed laminae being topped by clay clots (Fig. 7A –arrows-; S2 –arrows-). As the t9 slide is defined by a MB (Fig. 7A) we consequently translated the MB and L-MB feature (Figs. 4A; 5A; 7A) into sediment composition: in other words, we started considering the MB and L-MB equivalent to the presence of mixed lamina-*Coscinodiscus* lamina duplet. This deduction is confirmed by the investigations at higher magnifications of slides t13, t14, t9 images (800 x and 2000 x: Figs. 4B; 5B, 8A), where this duplet prevails. As the L-MB and MB are the mostly observed throughout the CLQ20 sample, we deduce that the mixed lamina-*Coscinodiscus* lamina duplet is the one most frequent in CLQ20.

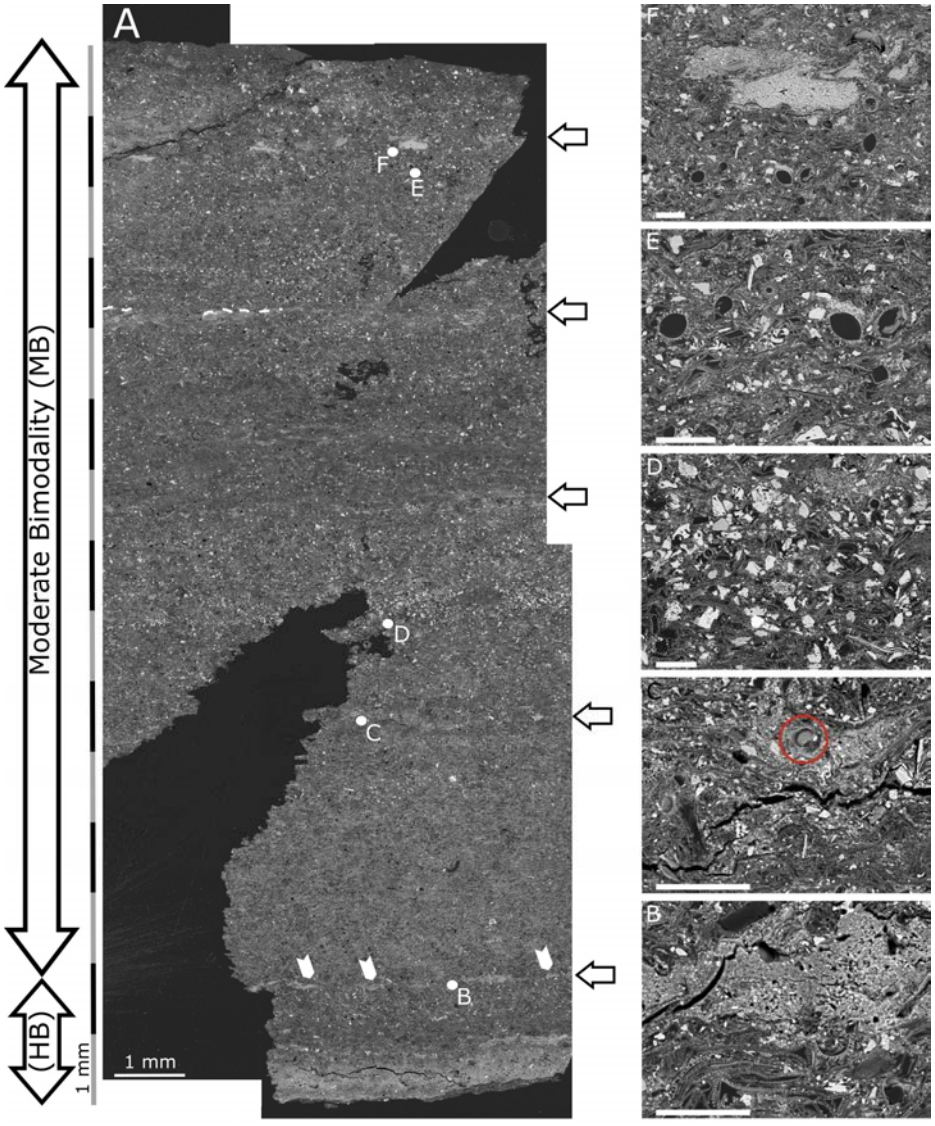

Fig. 7. BSE-SEM images of slide t9. A. Low magnification (100x) BSE image of slide t9, which is characterised at its bottom by a high bimodality, given by the contrast of a terrigenous lamina and the terrigenous boudinage-like top of a mixed lamina (arrowheads) with the overlying biogenic laminae (see Figs. 7B; 8A). The rest of the slide is characterised by moderate bimodality (MB) given by the sparse presence of silt particles in mixed laminae, which alternates with *Coscinodiscus* laminae (see Fig. S2) within a darker

matrix (diatomite). White arrows indicate the thin terrigenous boudinage-like top of the mixed laminae. The dotted line represents a continuous, straight but faint, upper boundary between the terrigenous top of a mixed lamina with a *Coscinodiscus* lamina. Letters highlights the position of images in the right column. B. Lower boundary of the terrigenous top of a mixed lamina. C. Detail of a diatom frustule (red circle) within the terrigenous top of the mixed lamina. D. Silt particles in a mixed lamina. E. *Stephanopyxis* frustules within a mixed lamina. F. Boudinage-like structure of the terrigenous top of a mixed lamina. Scale bars in 7B-F: 100 µm.

The mixed lamina-*Coscinodiscus* lamina duplet shows very different thicknesses, the three highlighted in Fig. 5B varying from ca. 875 µm to ca. 1750 mm, with a huge difference in the thickness of the two mixed laminae (ca. 375 µm in the second duplet vs. ca. 1500 µm in the third duplet). Differences in the thickness of *Coscinodiscus* laminae are nonetheless noteworthy: on one hand, the *Coscinodiscus* lamina of the second and third duplets are similar (varying from ca. 250 µm to 500 µm); on the other hand the *Coscinodiscus* lamina of the first (highlighted with an asterisk) and second duplets are ca. 1000 µm thick (Fig. 5B). The lower boundary of the mixed lamina of the first duplet is not clear, therefore we do not report the thickness of the whole duplet. Significantly, also in the duplet terrigenous lamina- *Coscinodiscus* lamina observed in Fig. 8A, the latter is ca. 250 µm as in the two cases in Fig. 5B; its terrigenous companion its ca. 650 µm thick (Fig. 8A), the thickness of the whole duplet being ca. 900 µm.

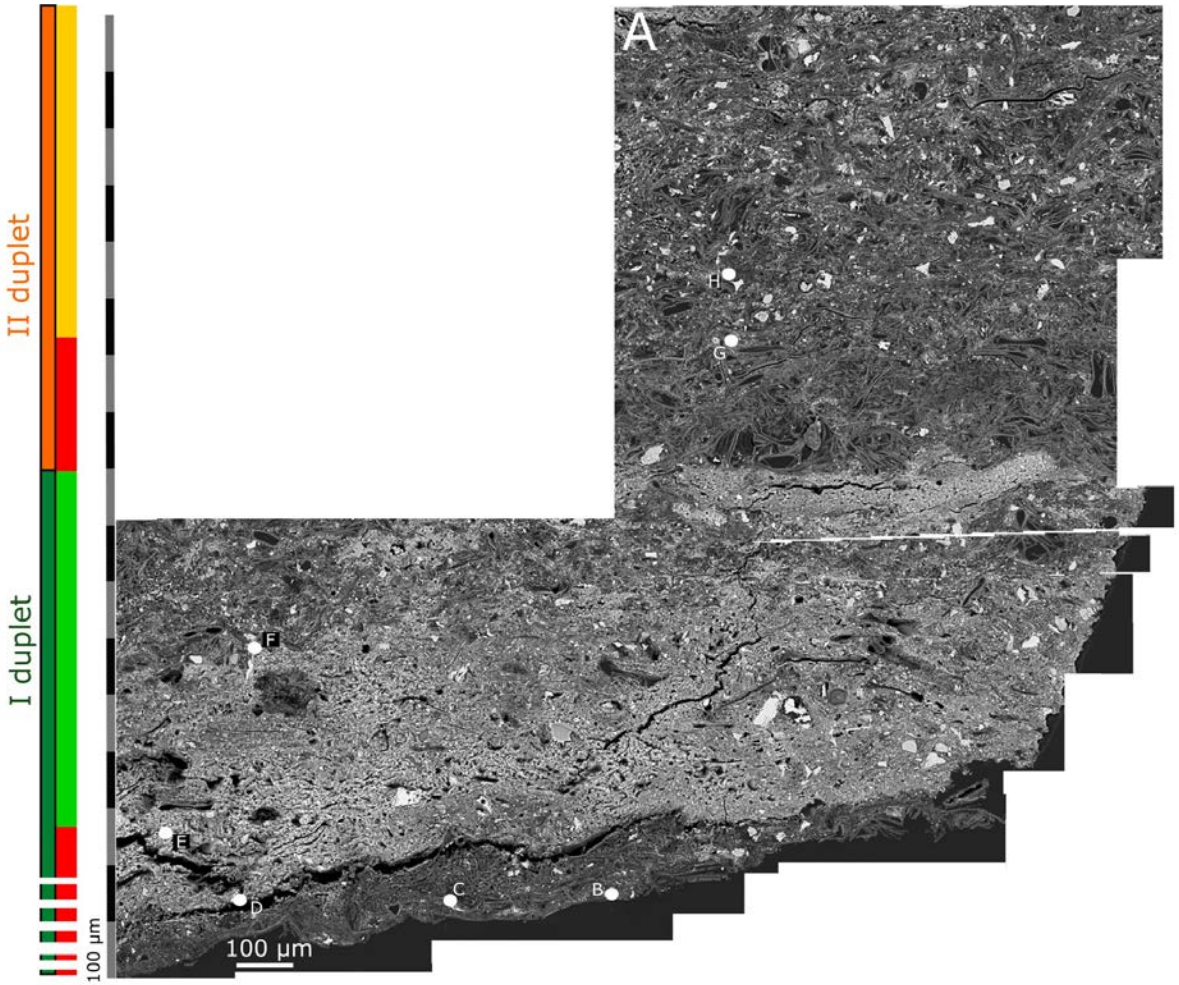

Figure 8 part I. BSE-SEM images of slide t9. A. High magnification (2000x) BSE image of the bottom of slide t9 (the same visible in Fig. 7A). Letters highlights the position of images in Fig 8 part II.

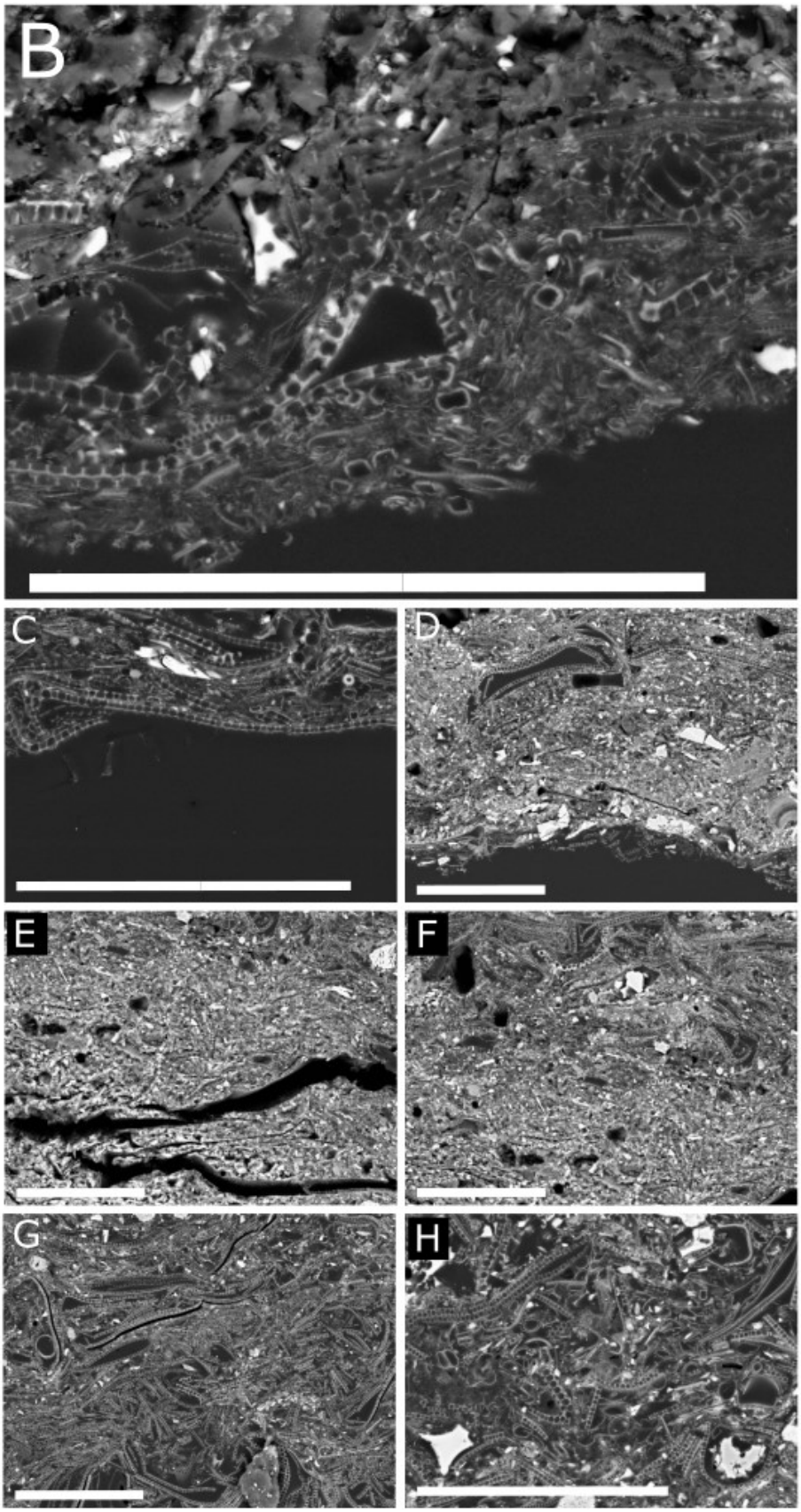

384

385 **Figure 8. part II. Details of slide t9. B. Details of *Thalassionema* specimen within a *Coscinodiscus* lamina. C. Silt particle within a**
386 ***Coscinodiscus* lamina. D. Detail of sparse diatom frustules within a terrigenous lamina. E. Detail of a terrigenous lamina. F.**
387 **Boundary between a terrigenous lamina with the overlying *Coscinodiscus* lamina. The boundary is wavy and interdigitated. G.**
388 **Boundary between a *Coscinodiscus* lamina with the overlying mixed lamina. The boundary is wavy, and faint, but continuous. H.**
389 ***Chaetoceros Hyalochaete* resting spores within a mixed lamina. Scale bars in 8B-H: 100 µm.**

4. Discussion

4.1. Paleoclimatic Implications of the Pisco Fm. Diatom Laminae

There are at least three features confirming that laminae in the CLQ20 sample are the product of a primary deposition process: i) the recurrent patterns of laminae in the CLQ20 sediments, in particular the mixed lamina-*Coscinodiscus* lamina; ii) the very well-defined boundaries of the terrigenous laminae; and iii) the lateral continuity of laminae.
The characteristic of the primary production inputs and of the terrigenous ones, can therefore be used as proxy for a paleoclimatic reconstruction of the area.

The studies of laminated sediments from the Peru forearc basins (Kemp, 1990; Brodie and Kemp, 1994) described upper Quaternary laminated sediments from the Peru shelf and upper slope. These were collected during ODP Exp 112 (Sites 680, 681 and 686) and during the R.R.S. Darwin Leg 38 (Sites 38.10 and 38.9). These studies highlighted the presence of three different groups of laminae; isolated, irregularly spaced and continuous sub-millimetre laminae. In all those three cases diatomaceous laminae are often mainly monospecific and composed of upwelling genera, such as *Skeletonema* and *Chaetoceros*. Conversely, *Coscinodiscus* oozes are rare. On the other hand, terrigenous laminae are either silt-rich (main thickness 600 μm, with a standard deviation of 350 μm) or clay-rich laminae (main thickness 550 μm, with a standard deviation of 500 μm), with the silt component not invariably present in the sequence (Brodie and Kemp, 1994). These laminae form a sub-millimetre couplet that is irregularly inter-laminated with diatom ooze. The oozes are controlled by the intensity of upwelling and/or the nutrient content of upwelled waters, while terrigenous laminae are the expression of regular rainfalls caused by the permanent presence of warm water off Peru during Isotope Stage 5 (Brodie and Kemp, 1994). The absence of diatom oozes between the silt/clay couplets is interpreted by the authors either as the result of absence of an algal bloom or the complete dissolution of the crop in the water column; both these hypotheses would suggest a reduction of nutrient availability, a feature which is consistent with El-Niño events (Brodie and Kemp, 1994).

Coscinodiscus spp. were associated with the "Fall dump" event, described for the first time in the Gulf of California, during the Holocene, by Kemp et al. (2000). The authors identify *Coscinodiscus* spp. specimens as "clusters of individuals rather than as contiguous sub-laminae" deposited above the diatomaceous laminae (made either of *Rhizosolenia* spp. or *Stephanopyxis palmeriana*) overlying the summer terrigenous lamina. Therefore, the authors include this genus among those that are able to thrive at the thermo/nutricline at low light conditions preferring a stratified water column, the so-called "shade" flora (Sournia, 1982; Kemp et al., 2000). Blooms of the "shade flora" may last throughout the periods of water stratification; the diatoms growing during this period start settling with the onset of fall/winter mixing (the "fall dump") (Kemp et al., 2000). These characteristics make them differ from the small subgenus *Chaetoceros Hyalochaete*, which thrives during upwelling conditions (spring) (Kemp et al. 2000). Somehow similarly, Romero and Hebbeln (2003), studying diatom assemblages of surface sediments below the Peru-Chile Current, list *Chaetoceros* species in the coastal upwelling group (together with *Thalassionema nitzschioides* var. *nitzschioides*), while they classify *Coscinodiscus argus* and *C. radiatus* in the coastal planktonic group (characterised by the presence of non-upwelling associated species). Yet, the authors find *C. argus* and *C. radiatus* together with *Chaetoceros* spp. between 34° and 38° S, highlighting that at those latitudes the primary production is due to both upwelling and proliferation of the fall dump flora during periods of water column stratification.

Following these observations, the huge contribution of *Coscinodiscus* spp. to the diatom fraction in laminae of sample CLQ20 and the scarce presence of *Chaetoceros Hyalochaete* spp.,

which was observed only in small sparse clusters (Figs. 4I, 8H), testify that primary production during the deposition of the F member was regulated by the stratification of the water column rather than by coastal upwelling; however, the presence of both phenomena in the same region, during different time of the year, is also plausible.

On one hand, the absence of *Rhizosolenia* spp. and *Stephanopyxis palmeriana* in the fall dump lamina suggests that the dominance of *Coscinodiscus* is not only related to stratification of the water column but also to some other ecological limiting factor. As *Stephanopyxis palmeriana* is known as a warm water (Drebes, 1966) tropical species (Molina et al., 1997), warmer than *Stephanopyxis turris* (Cupp, 1943), a species sporadically present in the CLQ20 sediments (Figs. 4B, I; 5B, L), it appears that water temperature may play a role in the absence of *S. palmeriana*. More generally, it can easily be assumed that the waters present in the Eastern Equatorial Pacific (EEP) Ocean during the late Miocene had different properties and origin in respect of those present in the Gulf of California during the Holocene; as such, it is not surprising that the dominant genera thriving at the thermocline in these two scenarios are different.

On the other hand, the absence of a strong upwelling, such as recorded in the laminae of the CLQ20 sample, may reflect a deepening of the thermocline in the EEP during the Messinian. Currently, this condition is registered during El Niño events: during the 1982-1983 El Niño, the winds were constantly upwelling-favourable but the thermocline was deeper than normal. Thus, as the source depth of upwelled water was the same of normal conditions (i.e. 50-100 m), upwelled waters were warm and poor of nutrients, as they came shallower than the thermocline (Huyer et al., 1987). Such a functioning of the El Niño was later confirmed by other authors (Strub et al., 1998; Hill et al., 1998).

With these observations in mind, when looking at the CLQ20 mosaics one may be tempted to say that the mixed lamina-*Coscinodiscus* lamina duplets, together with the terrigenous lamina – *Coscinodiscus* lamina duplets are not only the expression of a El-Niño like condition, but, indeed of the El Niño condition itself (or, at least, of a proto El-Niño condition). Not only the paucity of CRS, together with the abundance of *Coscinodiscus* ssp., highlights a stratified water column with warm and nutrient-poor upwelled water: also the presence of silt particles in mixed laminae point to a rainy condition, which appears to increase its intensity periodically (as it is known to happen during El Nino phenomena; see for examples Caviedes, 1984; Bull et al., 2000), leading to the formation of clots of clay (Figs. 7A –arrows-; Fig. S2 –arrows-). Although aware that such affirmation is far too reckless (more data would be needed for such a statement), we still think that this observation may encourage to start to look better into diatomaceous records that may help us comprehend when and how the ENSO phenomenon started.

At present the El Niño phenomenon has been identified back to the Cretaceous (Davies et al., 2012) and to the so called "Middle Pliocene Warm Period", ca. 4.5 – 3.0 Ma (MPWP, Fig. 3; Wara et al., 2005; Fedorov et al., 2006; Ravelo et al., 2006; Ragaini et al., 2008; White and Ravelo, 2020a, b. See Note2 in Suppl.Mat.). Some authors stated that, during the MPWP the El Niño conditions was permanent, rather than showing a periodicity similar to that of recent days: this is the so called "El Padre" state (Ravelo et al., 2014). The deepening of the thermocline and, therefore, the phenomena of El Niño and of El Padre, are triggered by the warming of the EEP and by the consequent drop of the temperature gradient between the Western Pacific Warm Pool (WPWP) and the EEP (Wara et al., 2005; Zhang et al., 2014a).

The hypothesis on whether the El Padre state either existed or is just a result of a bias in the proxies (TEX_{86}, $U^{K'}_{37}$, Mg/Ca, foraminiferal sea surface temperature trends) used for the reconstruction of the SST gradient is still ongoing (Zhang et al., 2014a, b; Ravelo et al., 2014; White and Ravelo 2020a, b, and reference therein), also extending into the Middle Miocene (Fox et al., 2021).

Although the discussion on the existence of an El Padre State lies outside the objectives of this paper, we would like to point out that: 1) there is no doubt that the CLQ20 *Coscinodiscus* laminae point to a deepening of the thermocline already in the Messinian. Yet, it is stunning to

observe that the deposition of CLQ20 happened during a period when SST in the EEP were as high as during the middle Pliocene warm period (Fig. 3); and 2) the BSE images of CLQ20 highlights that shade flora can represent a huge percentage of the total diatom assemblage; therefore, given the importance of the carbon export attributable to the thriving of the shade flora at depth, the use of biogenic silica as a proxy for intensification of upwelling, as done in some researches (for example, Holbourn et al., 2014; Fox et al., 2021; also Esperante et al., 2015 suggest that the abundant occurrence of *Thalassionema nitzschioides* in the sediment of the Pisco Fm. suggests strong upwelling conditions) should not be used without a quantitative check of the different diatom species present in the sediment.

We need to recall to the readers that the CLQ20 sample is a very short piece of the diatomite portion of the P2 allomember of the Pisco Fm and that it may be representative neither of the whole F member, nor of the diatomitic portions of the other older and younger allomembers of the Pisco Fm (Lamy et al., 2001, affirm that changes in continental rainfall in southern Chile are regulated by millennial to multi-centennial shifts in the position of the southern westerlies, periods that lag far behind the duration of the CLQ F member deposition). However, in their studies of the biostratigraphy of the Pisco Fm, Gariboldi et al., (2017) have published a table of relative abundances for all the diatom species encountered in the Cerro Los Quesos; from this work (table 3 of Gariboldi et al., 2017; see Note3 in Suppl.Mat.) we can infer that *Coscinodiscus asteromphalus* is present in great abundance in almost all the samples collected in the CLQ F member; yet, also CRS are always present. This apparent equality between these two genera abundances can be explained considering the counting method (Schrader and Gersonde, 1978; Armand, 1997; Crosta and Koç, 2007); following this protocol only *Coscinodicus* spp. valve which are preserved for ¾ or more can be counted in the assemblage. However, the higher valve-face diameter/pervalvar-axis ratio makes large diatoms easier to break during slide preparation, resulting at last in an underestimation of large diatoms in the assemblages. Conversely CRS are often found intact, with the 2 valves still connected.

As such, it appears clear that analyses on diatom assemblages by means of the light miscroscope, combined with those on diatom laminations, where possible, may be the most direct proxy, yet imprecise (as they give no absolute values on the reduced zonal SST gradient), to study the initiation and the temporal patterns of ENSO in the deep time and to verify the hypothesis of the El Padre state. On one hand, the observation of laminae in their original depositional settings gives a glimpse, not only on the depositional mechanism, but also on the real relative abundance of different species; on the other hand, light microscope analysis is essential to investigate long stratigraphic succession efficiently.

The significance of the *Actinoptychus* lamina (Figs. 6A, D, E) is yet to be understood. Sub-laminae have been described in other contexts (Maddison et al., 2006); however, we are not yet able to explain the ecological significance of the *Actinoptychus* lamina in the paleoclimatic context that we have just discussed.

4.2. The Role of Diatom Laminations in Preserving Marine Fossil Vertebrates

The investigation of diatomaceous laminae of the CLQ20 sample, the recognition of some laminae sequences that may be assumed as annual cycles (literally the mixed lamina- *Coscinodiscus* lamina and the terrigenous lamina-*Coscinodiscus* lamina duplets) and the possibility of measuring their thickness, open a further discussion on their role in favoring the preservation of marine fossils in the F member of the Pisco Fm at CLQ. The sedimentation rates registered along the F member (500 µm to 2 mm/a for the mixed lamina- *Coscinodiscus* lamina duplet, Fig. 5B; 900 µm for the terrigenous lamina –*Coscinodiscus* lamina duplet, Fig. 8A), although supported by few data, are conspicuously different from those calculated for the whole section at CLQ, at least doubling and sometimes even increasing of one order of magnitude those previously reported by Gariboldi et al, 2017 (0.2 mm/a of Gariboldi et al. 2017 for the CLQ section vs. 0.5 to 2 mm/a (50 to 200 cm/ka)

for the F member, this study). Differing from Gariboldi et al., (2017), who took in account a compaction of the sediments equal to 60% (by giving a wrong interpretation to Isaacs et al., 1983), in this paper we consider a definitely lower porosity loss for diatomaceous sediments due to compaction: Hamilton (1976) calculated a porosity loss during early burial of diatomaceous sediments equal to 15% (from 86% to 71% at 500 m below sea floor). Adding this 15% to the thickness of laminae observed in CLQ20 would implicate an insignificant increase to the yearly sedimentation rates. This implies that only in some cases these sedimentation rates are higher than those of Quaternary basins where primary production is high (e.g. Pleistocene of DSDP Site 478, Gulf of California, DSDP Leg 64, > 125 cm/ka, Schrader 1982; Quaternary of ODP Site 686, West Pisco Basin, ODP Leg 112, 16 cm/ka Suess and Von Huene 1988; Pleistocene of ODP Site 1078 outside the Bight of Angola, ODP Leg 175, 60 cm/ka, Wefer et al. 1998; Pleistocene of ODP Site 881, 5.6 cm/ka and Mio–Pliocene of ODP Site 883, 9.1 cm/ka, Subarctic Pacific Ocean, ODP Leg 145, Rea et al. 1993); to this list we add the sedimentation rates recorded in the last 2.6 ka old sediments of the Edisto Inlet, Ross Sea, Antarctica: Tesi et al. (2020) calculated a sedimentation rate equal to 2 to 7 mm/a (200 to 700 cm/ka) for the laminated diatomaceous sediment of core HLF17-01. As, due to their lithology and fabric, sediments of HLF17-01 may be considered a modern analogue of sediments from the F member, it is worth reporting that visual observations and preliminary analysis on the top meters of the HLF-17 revealed a soupy consistence of the sediments and a water content that was close to 90% (Tommaso Tesi personal communication; Karen Gariboldi personal observation). Imaging such physical characteristic for a just-deposed diatom ooze at the bottom of the East Pisco Basin would itself explain how deep marine vertebrate carcasses may have sunk into the sediments, supporting the "impact burial" (partial or complete burial of an object in the sediments upon its high velocity sinking through the water column into soupy substrates) hypothesis proposed by Bosio et al. (2021b) to explain the rapid burial of marine vertebrates in the Pisco Fm. Indeed, any of the sedimentation rates calculated in this paper and in Gariboldi et al., 2017 are not high enough to cover large carcasses permitting high articulation and high completeness of the fossil specimens, as observed in the Pisco Fm (Gariboldi et al., 2015). As such, we agree with Brand et al. (2004), who state that rapid burial is needed to explain such a preservation in the Pisco Fm. However, we disagree when they state that "such burial requires diatom accumulation rates at least three to four orders of magnitude faster than is usual in the ocean today—centimeters per week or month, rather than centimeters per thousand years". Also, Gariboldi et al. (2015) highlighted the role of dolomite precipitation inside and outside (dolomite nodule) the whale carcasses in the process of preservation of the fossils. The process of dolomite precipitation, which also includes recurrent basin-wide decimetric-thick dolomite layers (Malinverno et al., accepted), was explained as biomediated by sulphate-reducing bacteria, which are able to degrade organic matter in low-oxygen environment, as demonstrated also in laboratory experiments (see references therein Gariboldi et al. 2015). Thus, the sinking of the carcasses into the soupy diatom ooze would have favored the formation of the Pisco Lagerstätte also by subtracting the carcasses from a possible oxygenated sea floor, thus favoring dolomite precipitation.

5. CONCLUSIONS

Backscattered electron imagery analysis of Cerro Los Quesos laminated diatomaceous mudstone provided insight into the seasonality that was affecting water column stability.

The most frequent laminae duplet observed in the Messinian CLQ20 sample is the mixed lamina – *Coscinodiscus* lamina duplet. The large contribution of this duplet and of the genus *Coscinodiscus* in general (also in the less frequent terrigenous lamina – *Coscinodiscus* lamina duplet) in the CLQ20 sediments, together with the paucity of, reflects a rather deep position of the thermocline. This water column setup led to a weak proliferation of upwelling related diatom species (i.e., *Chaetoceros Hyalochaete* and *Thalassionema*), as the upwelled waters were warm and nutrient-poor. Such oceanographic situation resembles that hypothesized for the so-called "El Padre

state" in the middle Pliocene Warm Period; this is described as a constant El Niño phenomenon triggered by the warming of the EEP and the consequent drop of the temperature gradient between the WPWP and the EEP itself. As such, we highlight that studies focused on verifying the existence of the El Padre setup in the low latitude Pacific during the Late Miocene are needed.

Also, analyses on CLQ20 laminae thickness have confirmed that sedimentation rates in the Pisco Basin during the Late Miocene were comparable to those of Quaternary basins elsewhere. This evidence rules out the hypothesis that depositions of diatomites in the East Pisco Basin were orders magnitude faster than in today's oceans. Moreover, direct observation on modern diatom oozes and the observation made on their water content, make us affirm that the hypothesis of an "impact burial" for the marine vertebrate carcasses is robust.

On a broader view, our study suggests that:

- during diatom counts for palaecological analysis, special care should be paid in not underestimating large-sized diatoms over small-sized ones; light microscope analysis coupled with BSEI analysis on diatom laminations (where possible) helps overcome this possible bias;
- analyses on diatom assemblages and diatom laminations, where possible, may be the most direct proxy, yet imprecise (as it gives no absolute values on the reduced zonal SST gradient), to study ENSO in the deep time;
- the use of biogenic silica as a proxy for intensification of upwelling, as done in some researches, should be used with caution, given the importance of the carbon export attributable to the thriving of the shade flora at depth.

ACKNOWLEDGMENTS

We would like to thank Anthony Oldroy, Peter Fisher, Lindsey Axe and Duncan Muir (School of Earth and Ocean Sciences, Cardiff University) for the help during sample preparation and SEM analyses. We would also like to thank Prof. John Barron for his constant support and for the many productive discussions. This study was supported by grants from the Italian Ministero dell'Istruzione dell'Università e della Ricerca (PRIN Project 2012YJSBMK to G. Bianucci), by a National Geographic Society Committee for Research Exploration grants (9410-13 to G. Bianucci), and the University of Camerino (FAR 2019, STI000102 to C. Di Celma). K.G. would like to thank Caterina Morigi, Alessandra Negri and Giacomo Galli for their help in improving the manuscript.

REFERENCES

- Alley K., Patacca K., Pike J., Dunbar R., Leventer, A., (2018). Iceberg Alley, East Antarctic Margin: Continuously laminated diatomaceous sediments from the late Holocene. *Marine Micropaleontology*, 140, 56-68.
- Armand L., (1997). The use of diatom transfer functions in estimating sea-surface temperature and sea-ice in cores from the southeast Indian Ocean. Ph.D thesis, Australian National University, Canberra, Australia.
- Bianucci G., Di Celma C., Landini W., Post K., Tinelli C., de Muizon C., Gariboldi K., Malinverno. E., Cantalamessa G., Gioncada. A., Collareta A., Salas-Gismondi R., Varas-Malca R., Urbina M. & Lambert O., (2016a). Distribution of fossil marine vertebrates in Cerro Colorado, the type locality of the giant raptorial sperm whale Livyatanmelvillei (Miocene, Pisco Formation, Peru). *Journal of Maps*, *12*(3), 543-557.
- Bianucci G., Di Celma C., Collareta A., Landini W., Post K., Tinelli C., de Muizon C., Bosio G., Gariboldi K., Gioncada A., Malinverno E., Cantalamessa G., Altamirano-Sierra A., Salas-Gismondi R., Urbina M. & Lambert O., (2016b). Fossil marine vertebrates of Cerro Los Quesos:

643 distribution of cetaceans, seals, crocodiles, seabirds, sharks and bony fish in a late Miocene
644 locality of the Pisco Basin, Peru. *Journal of Maps*,12(5): 1037-1046
645 -Bosio G., Gioncada A., Gariboldi K., Bonaccorsi E., Collareta A., Pasero M., Di Celma C.,
646 Malinverno E., Urbina M., Bianucci G., (2021a). Mineralogical and geochemical
647 characterization of fossil bones from a Miocene marine Konservat-Lagerstätte. *Journal of South*
648 *American Earth Sciences*, 105, 102924.
649 - Bosio G., Collareta A., Di Celma C., Lambert O., Marx F. G., de Muizon C., Gioncada A.,
650 Gariboldi K., Malinverno E., Varas-Malca R., Urbina M, Bianucci G., (2021b). Taphonomy of
651 marine vertebrates of the Pisco Formation (Miocene, Peru): Insights into the origin of an
652 outstanding Fossil-Lagerstätte. *Plosone*, 16(7), e0254395.
653 - Brand L.R., Esperante R., Chadwick A.V., Poma Porras O., Alomía M., (2004). Fossil whale
654 preservation implies high diatom accumulation rate in the Miocene-Pliocene Pisco Formation of
655 Peru. *Geology*, 32(2): 165-168.
656 - Brodie I., Kemp A.E.S., (1994). Variation in biogenic and detrital fluxes and formation of laminae
657 in late Quaternary sediments from the Peruvian coastal upwelling zone. *Marine Geology*, 116:
658 385-398.
659 -Bull D., Kemp A.E.S., Weedon G.P.A, (2000). 160-k.y.-old-record of El Niño southern Oscillation
660 in marine production and coastal run-off from Santa Barbara Basin, California, USA. *Geology*,
661 28, 1007-1010.
662 - Caviedes C. N., (1984). El Nino 1982-83. *Geographical Review*, 267-290.
663 - Collareta A., Landini W., Lambert O., Post K., Tinelli C., Di Celma C., Panetta D., Tripodi M.,
664 Salvadori P.A., Caramella D., Marchi D., Urbina M., Bianucci G., (2015). Piscivory in a
665 Miocene CetotheriidaeofPeru: first record of fossilised stomach content for an extinct baleen-
666 bearingwhale. *Science of Nature*, 102, 70.
667 - Collareta A., Lambert O., Marx F. G., de Muizon C., Varas-Malca R., Landini W., Bosio G.,
668 Malinverno E., Gariboldi K., Gioncada A., Urbina M., Bianucci G., (2021). Vertebrate
669 Palaeoecology of the Pisco Formation (Miocene, Peru): Glimpses into the Ancient Humboldt
670 Current Ecosystem. *Journal of Marine Science and Engineering*, 9(11), 1188.
671 - Corselli C., Principato M.S., Maffioli P., Crudeli D., (2002). Changes in planktonic assemblages
672 during sapropel S5 deposition: Evidence from Urania Basin area, eastern Mediterranean.
673 *Paleoceanography*, 17(3): 1-30.
674 - Crosta X., Koç N., (2007) – Chapter Eight Diatoms: From Micropaleontology to Isotope
675 Geochemistry. *Developments in Marine Geology*, Volume 1, pp. 327-369.
676 - Cupp E.E., (1943). Marine plankton diatoms of the west coast of North America. Otto Koeltz
677 Science Publishers.
678 - Drebes G., (1966). On the life history of the marine plankton diatom *Stephanopyxis*
679 *palmeriana*. *Helgoländer wissenschaftliche Meeresuntersuchungen*, *13*(1), 101-114.
680 - Davies A., Kemp A.E., (2016). Late Cretaceous seasonal palaeoclimatology and diatom
681 palaeoecology from laminated sediments. *Cretaceous Research*, *65*, 82-111.
682 -Davies A., Kemp A.E., Pike J., (2009). Late Cretaceous seasonal ocean variability from the
683 Arctic. *Nature*, *460*(7252), 254-258.
684 -Davies A., Kemp A.E., Weedon G.P., Barron, J.A., (2012). El Niño–southern oscillation variability
685 from the late cretaceous Marca shale of California. *Geology*, *40*(1), 15-18.
686 - Di Celma C., Malinverno E., Cantalamessa G., Gioncada A., Bosio G., Villa I.M., Gariboldi K.,
687 Rustichelli A., Pierantoni P.P., Landini W., Tinelli C., Collareta A., Bianucci G., (2016).
688 Stratigraphic framework of the late Miocene Pisco Formation at Cerro Los Quesos (Ica Desert,
689 Peru). *Journal of Maps*, 12(5): 1020-1028.
690 - Dudley W.C., Blackwedler P., Brand L., Duplessy J.-C., (1986). Stable isotopic composition of
691 coccoliths. *Marine Micropaleontology*, 10(1-3):1–8

- Dunbar R.B., Berger W.H., (1981). Fecal pellet flux to modern bottom sediment of Santa Barbara Basin (California) based on sediment trapping. *Geological Society of America Bulletin* 92(4): 212-218.
- Esperante R., Brand L., Nick K., Poma O., Urbina M., 2008. Exceptional occurrence of fossil baleen in shallow marine sediments of the Neogene Pisco Formation, Southern Peru. *Palaeogeography. Palaeoclimatology. Palaeoecology*, 257:344–360.
- Esperante R., Brand L.R., Chadwick A.V., Poma O., (2015).Taphonomy and paleoenvironmental conditions of deposition of fossil whales in the diatomaceous sediments of the Miocene/Pliocene Pisco Formation, southern Peru - A new fossil-lagerstätte. *Palaeogeography, Palaeoclimatology, Palaeoecology*, 417:337–370.
- Fox L.R., Wade B.S., Holbourn A., Leng M.J., Bhatia R., (2021). Temperature gradients across the Pacific Ocean during the middle Miocene. *Paleoceanography and Paleoclimatology*, e2020PA003924.
- Fedorov A.V., Dekens P.S., McCarthy M., Ravelo A.C., DeMenocal P.B., Barreiro, M., Pacanowski R.C., Philander S.G., (2006). The Pliocene paradox (mechanisms for a permanent El Niño). Science, 312(5779), 1485-1489.
- Gariboldi K., Gioncada A., Bosio G., Malinverno E., Di Celma C., Tinelli C., Cantalamessa G., Landini W., Urbina M., Bianucci G., (2015). The dolomite nodules enclosing fossil marine vertebrates in the East Pisco Basin, Peru: field and petrographic insights into the Lagerstätte formation. *Palaeogeography, Palaeoclimatology, Palaeoecology*, 438, 81-95.
-Gariboldi K., Bosio G., Malinverno E., Gioncada A., Di Celma C., Villa I.M., Urbina M., Bianucci G., (2017). Biostratigraphy, geochronology and sedimentation rates of the upper Miocene Pisco Formation at two important marine vertebrate fossil-bearing sites of southern Peru. *Newsletters on Stratigraphy*, 50(4), 417-444.
- Gioncada A., Collareta A., Gariboldi K., Lambert O., Di Celma C., Bonaccorsi E., Urbina M., Bianucci G., (2016). Inside baleen: exceptional microstructure preservation in a late Miocene whale skeleton from Peru. *Geology*, 44(10), 839-842.
- Gioncada A., Gariboldi K., Collareta A., Di Celma C., Bosio G., Malinverno E., Lambert O., Pike J., Urbina M., Bianucci G., (2018a). Looking for the key to preservation of fossil marine vertebrates in the Pisco Formation of Peru: new insights from a small dolphin skeleton. *Andean Geology*, 45.3 (2018):379-398.
- Gioncada A., Petrini R., Bosio G., Gariboldi K., Collareta A., Malinverno E., Bonaccorsi E., Di Celma C., Pasero M., Urbina M., Bianucci G., (2018b). Insights into the diagenetic environment of fossil marine vertebrates of the Pisco Formation (late Miocene, Peru) from mineralogical and Sr-isotope data. *Journal of South American Earth Sciences*, *81*, 141-152.
- Grigorov I., Pearce R.B., Kemp A.E.S., (2002). Southern Ocean laminated diatom ooze: mat deposits and potential for palaeo-flux studies, ODP leg 177, Site 1093. *Deep-Sea Research*, 49, 3391-3407.
- Grimm K.A., Lange C.B., Gill A.S., (1996). Biological forcing of hemipelagic sedimentary laminae; evidence from ODP Site 893, Santa Barbara Basin, California. *Journal of Sedimentary Research*, 66(3), 613-624.
- Hamilton E.L., (1976). Variations of density and porosity with depth in deep-sea sediments. *Journal of Sedimentary Research*, *46*(2), 280-300.
- Hill A.E., Hickey B.M., Shillington F.A., Strub P.T., Brink K.H., Barton E.D., and Thomas A.C., (1998), Eastern Ocean boundaries. In *The Sea*, vol. 11, edited by A. R. Robinson and K. H. Brink, pp. 29– 67, John Wiley and Sons Edition, NY.
- Holbourn A., Kuhnt W., Lyle M., Schneider L., Romero O., Andersen, N., (2014). Middle Miocene climate cooling linked to intensification of eastern equatorial Pacific upwelling. *Geology*, 42(1), 19-22.
- Huyer A., Smith R.L., Paluszkiewicz T., (1987). Coastal upwelling off Peru during normal and El Niño times, 1981–1984. *Journal of Geophysical Research: Oceans*, 92(C13), 14297-14307.

- Isaacs C.M., Pisciotto K.A., Garrison R.E., (1983). Facies and diagenesis of the Miocene Monterey Formation, California: a summary. *Developments in Sedimentology*, 36: 247-282.
- Kemp A.E.S., (1990). Sedimentary fabrics and variation in lamination style in Peru continental margin upwelling sediments. *Proceedings of ODP, Scientific Results*, 112, 43-58.
- Kemp A.E.S., Pearce R.B., Koizumi I., Pike J., Rance S.J., (1999). The role of mat-forming diatoms in formation of the Mediterranean sapropels. *Nature*, 398, 57-61.
- Kemp A.E.S., Pike J., Pearce R.B., Lange C.B., (2000). The "Fall dump"-a new perspective on the role of a "shade flora" in the annual cycle of diatom production and export flux. *Deep-Sea Research II*, 47: 2129-2154.
- Lambert O., Bianucci G., Post K., de Muizon C., Salas-Gismondi R., Urbina M., Reumer J., (2010). The giant bite of a new raptorial sperm whale from the Miocene epoch of Peru. *Nature*, 466(7302), 105.
- Lamy, F., Hebbeln, D., Röhl, U., & Wefer, G., (2001). Holocene rainfall variability in southern Chile: a marine record of latitudinal shifts of the Southern Westerlies. *Earth and Planetary Science Letters*, 185(3-4), 369-382.
- Maddison E.J., Pike J., Leventer A., Dunbar R., Brachfeld S., Domack E.W., Manley P., McClennen C., (2006). Post-glacial seasonal diatom record of the Mertz Glacier Polynya, East Antarctica. *Marine Micropaleontology*, 60(1), 66-88.
- Maddison E.J., Pike J., Dunbar R., (2012). Seasonally laminated diatom-rich sediments from Dumont d'Urville trough, East Antarctic margin: Late-holocene neoglacial sea-ice conditions. *The Holocene*, 22(8), 857-875.
- Malinverno E., Bosio G., Gioncada A., Cimò R., Andò S., Mariani L., Coletti G., Boschi C., Gariboldi K., Galimberti L., Bianucci G., Urbina M., Di Celma C., (accepted). Laterally-continuous dolomite layers of the Miocene Pisco Formation (East Pisco Basin, Peru): a window into past cyclical changes of the diagenetic environment. Available at *SSRN*: https://ssrn.com/abstract=4170594 or http://dx.doi.org/10.2139/ssrn.4170594.
- Marty R., (1988). Stratigraphy and chemical sedimentology of Cenozoic biogenic sediments from the Pisco and Sechura Basins, Peru. PhD Thesis, Huston, Texas, Rice University.
- Marx, F.G., Uhen, M.D., (2010). Climate, critters, and cetaceans: Cenozoic drivers of the evolution of modern whales. *Science*, *327*(5968), 993-996.
- Molina R.E., Manrique, F.A., García J., (1997). Nota sobre un florecimiento de *Stephanopyxis palmeriana* (Greville) Grunow (Bacillariophyceae) en la bahía Kun Kaak, Golfo de California. *Hidrobiológica*, *7*(1), 84-86.
- Palmer A.A., Austin J.A. Jr., Schlager W., (1986). Introduction and explanatory notes. *Proceedings of ODP, Scientific Results*, 101, 5-23.
- Pike J., Kemp A.E.S., (1996a). Preparation and analysis techniques for studies of laminated sediments. In: *Palaeoclimatology and Palaeooceanography from laminated sediments*, ed. by A.E.S. Kemp, No°116: 37-48. Geological Society Special Publication, London.
- Pike J., Kemp A.E.S., (1996b). Records of seasonal flux in Holocene laminated sediments, Gulf of California. In: *Palaeoclimatology and Palaeooceanography from laminated sediments*, ed. by A.E.S. Kemp, No°116: 157-170. Geological Society Special Publication, London.
- Pike J., Kemp A.E.S., (1997). Early Holocene decadal-scale ocean variability recorded in Gulf of California laminated sediments. *Paleoceanography*, 12(2): 227-238.
- Pike J., Kemp A.E.S., (1999). Diatom mats in Gulf of California sediments: Implication for the paleoenvironmental interpretation of laminated sediments and silica burial. *Geology*, 27(4): 311-314.
- Pike J., Bernhard J.M., Moreton S.G., Butler I.B., (2001). Microbioirrigation of marine sediments in dysoxic environments: implications for early sediment fabric and diagenetic processes. *Geology*, 29 (10): 923-926.
- Pike J., Stickley C.E., (2013). Diatom fossil record from marine laminated sediments. In: *Encyclopedia of Quaternary Science*, ed. By S. Elias, C. Mock, Vol. 1: 554-561.

- Pilskaln C.H., Pike J. (2001). Formation of Holocene sedimentary laminae in the Black Sea and the role of the benthic flocculent layer. *Paleoceanography*, 16, 1-19.
- Ragaini L., Di Celma C., Cantalamessa G., (2008). Warm-water mollusc assemblages from northern Chile (Mejillones Peninsula): new evidence for permanent El Niño-like conditions during Pliocene warmth? *Journal of the Geological Society*, London, 165, 1075–1084.
- Ravelo A.C., Deken P. S., McCarthy M., (2006). Evidence for El Niño-like conditions during the Pliocene. *Gsa Today*, 16(3), 4.
- Ravelo A.C., Lawrence K.T., Fedorov A., Ford H.L., (2014). Comment on "A 12-million-year temperature history of the tropical Pacific Ocean". *Science*, *346*(6216), 1467.
- Rea, D. K., Basov, I. A., Janecek, T. R., Palmer-Julson, A. et al., (1993). *Proceedings of the Ocean Drilling Program, Initial Reports*, 145, 9–33.
- Romero O., Hebbeln D., (2003). Biogenic silica and diatom thanatocoenosis in surface sediments below the Peru–Chile Current: controlling mechanisms and relationship with productivity of surface waters. *Marine Micropaleontology*, 48(1-2), 71-90.
- Rousselle G., Beltran C., Sicre M.A., Raffi I., De Rafelis M., (2013). Changes in sea-surface conditions in the Equatorial Pacific during the middle Miocene–Pliocene as inferred from coccolith geochemistry. *Earth and planetary science letters*, 361, 412-421.
- Sancetta C., (1995). Diatoms in the Gulf of California: seasonal flux patterns and the sediment record for the last 15,000 years. *Paleoceanography*, 10 (1): 67-84.
- Schrader H., (1982). Diatom biostratigraphy and laminated diatomaceous sediments from the Gulf of California Deep Sea Drilling Project Leg 64. In Curray, J.R., More, D.G., Kelts, K., Einsele, G. *Proceedings of the Ocean Drilling Program*, Part A: Initial Reports 64(2), p. 1089-1116.
- Schrader H.J., Gersonde R., (1978). Diatoms and silicoflagellates. In: Zachariasse A., Riedel W.R., Sanfilippo A., Schmidt R.R., Brolsma M.J., Schrader H.J., Gersonde R., Drooger M.M., Broekman J.A. (Editors), Micropaleontological counting methods and techniques — An exercise on an eight meters section of the Lower Pliocene of Capo Rossello, Sicily. *Utrecht Micropaleontology Bulletin*, 17, 129–176
- Suess E., von Huene R. et al., (1988). *Proceeding of the Ocean Drilling Program, Initial Reports 112*. College Station, TX (Ocean Drilling Program).
- Sournia A., (1982). Is there a shade flora in the marine plankton? *Journal of Phytoplankton Research*, 4: 391-399.
- Stickley C.E., Pike J., Leventer A., Dunbar R., Domack E.W., Brachfeld S., Manley P., McClennan C., (2005). Deglacial ocean and climate seasonality in laminated diatom sediments, Mac. Robertson Shelf, Antarctica. *Palaeogeography, Palaeoclimatology, Palaeoecology*, 227(4), 290-310.
- Strub P.T., Mesías J.M., Montecino V., Rutllant J., Salinas S., (1998). Coastal Ocean Circulation off Western South America, Coastal Segment. In: Robinson, A.R., Brink, K.H. (Editors), *The Sea*, Volume 11. The Global Coastal Ocean, Regional Studies and Synthesis. Wiley, New York, pp. 273-313.
- Tesi T., Belt S.T., Gariboldi K., Muschitiello F., Smik L., Finocchiaro F., Giglio F., Colizza E., Gazzurra G., Giordano P., Morigi C., Capotondi L., Nogarotto A., Köseoğlu D., Di Roberto A., Gallerani, A., Langone, L., (2020). Resolving sea ice dynamics in the north-western Ross Sea during the last 2.6 ka: From seasonal to millennial timescales. *Quaternary Science Reviews*, 237, 106299.
- Thunell R., Pride C., Tappa E., Muller-Karger F., (1993). Varve formation in the Gulf of California: insights from time series sediment trap sampling and remote sensing. *Quaternary Science Reviews*, 12: 451-464.
- Wara M.W., Ravelo A.C., Delaney M.L., (2005). Permanent El Niño-like conditions during the Pliocene warm period. *Science*, 309(5735), 758-761.

- Wefer G., Berger W.H., Richter C., (1998). The Angola-Benguela upwelling system: paleoceanography synthesis of shipboard results from LEG 1751. In *Proceeding of the Ocean Drilling Program*, Initial Reports. 175. Texas A&M University, College Station, Texas.
- White S.M., Ravelo A.C., (2020a). Dampened El Niño in the early Pliocene warm period. *Geophysical Research Letters*, 47(4), e2019GL085504.
- White S.M., Ravelo A.C., (2020b). The benthic B/Ca record at Site 806: new constraints on the temperature of the West Pacific Warm Pool and the "El Padre" state in the Pliocene. *Paleoceanography and Paleoclimatology*, 35(10), e2019PA003812.
- Zhang Y.G., Pagani M., Liu Z., (2014a). A 12-million-year temperature history of the tropical Pacific Ocean. *Science*, 344(6179), 84-87.
- Zhang Y.G., Pagani M., Liu Z., (2014b). Response to Comment on "A 12-million-year temperature history of the tropical Pacific Ocean". *Science*, 346(6216), 1467-1467.

SUPPLEMENTARY MATERIAL

Note1: see Bianucci et al., 2016b and Di Celma et al., 2016 to compare the stratigraphic position of fossils and tephra; Di Celma et al. 2016 have investigated a 100 m longer section with M58 placed at ca. 267 m abs in their work)

Note2: before 2009 the Gelasian was placed in the Pliocene. Therefore, before 2009 the middle Pliocene warm period was identified as the early Pliocene warm period.

Note3: Gariboldi et al., 2017 take in consideration the stratigraphic section of Di Celma et al. 2016, not that of Bianucci et al. 2016. As such, in Di Celma et al., 2016, and in Gariboldi et al., 2017, the fossil whale M58 and sample CLQ20 are placed at ca. 267 m abs (rather than at 167.0 m abs, as stated in paragraph 2).

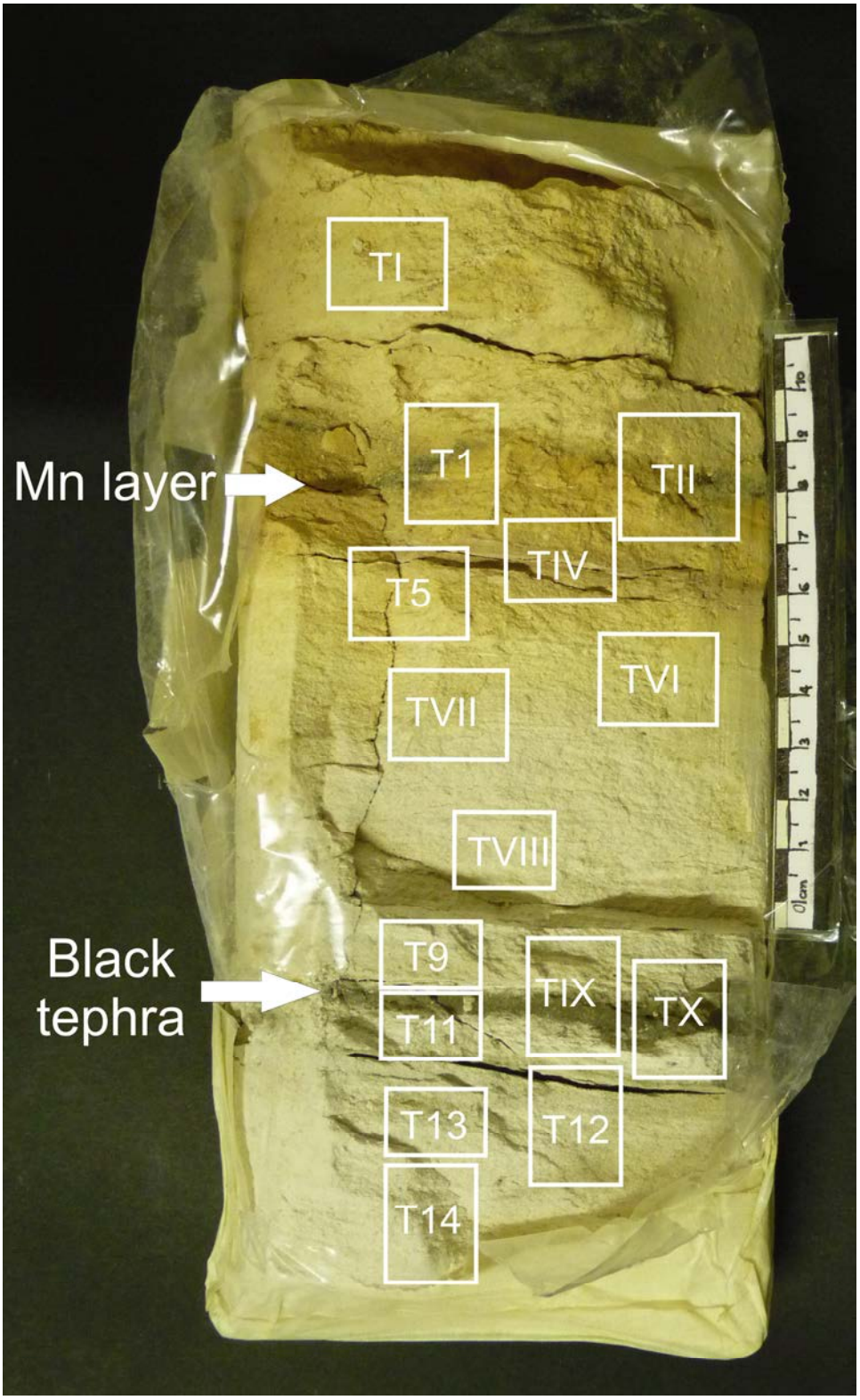

Figure S1. CLQ20 Sample. Positions of the thin sections along. Arrows indicate the Mn layer and the black tephra.

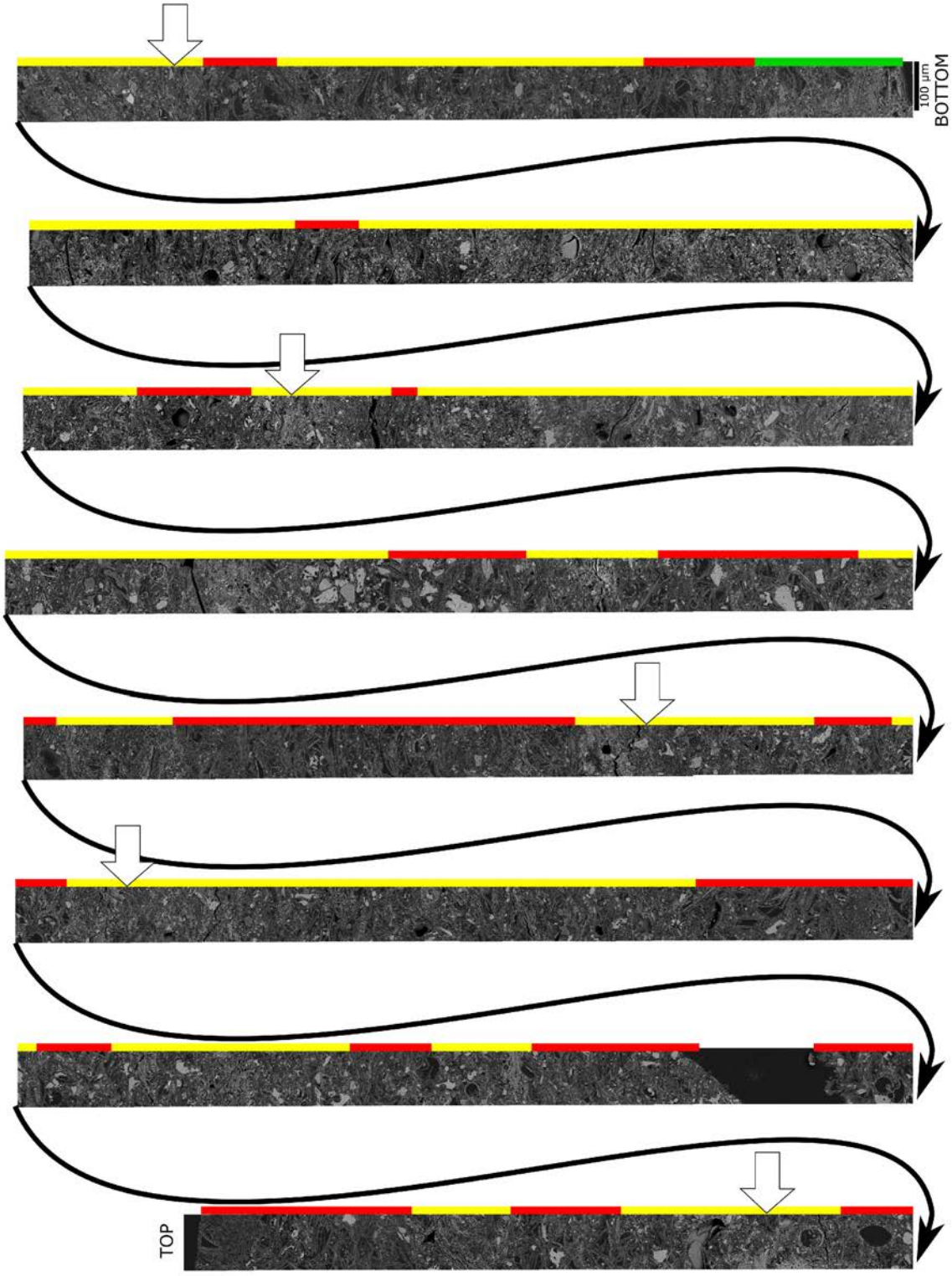

Figure S1. Composite BSE-SEM image of slide t9. This mosaic represents the t9 slide for all its length (1.5 cm), but only a very small portion of its width (ca. 110 µm vs ca. 2 cm at its widest point). This mosaic shows the periodicity of the *Coscinodiscus* laminae. Observe the mosaic from the bottom to the top of the columns, from the bottom right angle to the top left angle, following the black arrows. The small repetition of the images between the top of a column and the bottom of the following is needed to create the BSE mosaic manually. Green: terrigenous lamina; red: *Coscinodiscus* lamina; yellow: mixed lamina. The white arrows on the left of the columns correspond to those in Fig. 7A, highlighting the terrigenous tops of the mixed laminae. The interval with no colour corresponds to a crack in the thin section.